arXiv:1601.06718v2 [math.PR] 2 Feb 2016

Second order analysis of geometric functionals of Boolean models

Daniel Hug, Michael A. Klatt, Günter Last, Matthias Schulte

Abstract This paper presents asymptotic covariance formulae and central limit theorems for geometric functionals, including volume, surface area, and all Minkowski functionals and translation invariant Minkowski tensors as prominent examples, of stationary Boolean models. Special focus is put on the anisotropic case. In the (anisotropic) example of aligned rectangles, we provide explicit analytic formulae and compare them with simulation results. We discuss which information about the grain distribution second moments add to the mean values.

1 Introduction

In this article we study a large class of functionals of the Boolean model, a fundamental benchmark model of stochastic geometry [6, 39, 34] and continuum percolation [9, 31]. It has many applications in material science [44], physics [1, 40], and astronomy [27, 18], as well as, for the measurement of biometrical data [29] or the estimation of percolation thresholds [30, 28]. Intuitively speaking, a Boolean model is a collection of overlapping random grains, scattered in space in a purely

Daniel Hug
Karlsruhe Institute of Technology, Institute of Stochastics, D-76128 Karlsruhe, e-mail: daniel.hug@kit.edu

Michael A. Klatt
Karlsruhe Institute of Technology, Institute of Stochastics, D-76128 Karlsruhe, e-mail: michael.klatt@kit.edu

Günter Last
Karlsruhe Institute of Technology, Institute of Stochastics, D-76128 Karlsruhe, e-mail: guenter.last@kit.edu

Matthias Schulte
Karlsruhe Institute of Technology, Institute of Stochastics, D-76128 Karlsruhe, e-mail: matthias.schulte@kit.edu

random manner. This random object is defined as follows. Let $X = \{X_1, X_2, \ldots\}$ be a stationary Poisson process of intensity γ in $\mathbb{R}^n$, that is, a countable collection of random points in $\mathbb{R}^n$ such that the numbers of points in disjoint sets are independent and the number of points in each set follows a Poisson distribution whose parameter is γ times the Lebesgue measure of the set. Let $(Z_i)_{i\in\mathbb{N}}$ be a sequence of independent and identically distributed random convex bodies (nonempty compact convex subsets of $\mathbb{R}^n$), independent of X. The Boolean model Z is the random closed set defined by

$$Z := \bigcup_{i\in\mathbb{N}} (Z_i + X_i),$$

where $Z_i + X_i := \{z + X_i : z \in Z_i\}$. An example is the spherical Boolean model, where the Z_i are balls with random radii centred at the origin and $Z_i + X_i$ is the corresponding ball centred at X_i.

In this paper we study geometric functionals of the Boolean model Z. Prominent examples of such functionals are the intrinsic volumes (Minkowski functionals) and Minkowski tensors, which are efficient shape descriptors that have been successfully applied to a variety of physical systems [42]. (In [43], the different approaches and notations in the physics and mathematics literature are compared.). We are interested in the second order properties of the random variables obtained by applying geometric functionals to the restriction $Z \cap W$ of the Boolean model to a convex observation window $W \subset \mathbb{R}^n$. For a stationary and isotropic Boolean model, Miles [32] and Davy [7] obtained explicit formulae expressing the mean values of the Minkowski functionals in terms of the intensity and geometric mean values of the typical grain (see also [6, 39]). For mean value formulae for more general functionals in Boolean models we refer to [14]. We shall discuss here formulae for asymptotic covariances as well as multivariate central limit theorems for an increasing observation window. Much of the presented theory is taken from [16]. However, some results are new. In particular this is the first paper providing explicit covariance formulae involving the Euler characteristic of planar non-isotropic Boolean models. Our methods are based on the Fock space representation of Poisson functionals from [21] and the Stein-Malliavin approach to their normal approximation [35, 22, 23]. A completely different treatment of second moments of curvature measures of an isotropic Boolean model with an interesting application to morphological thermodynamics was presented in [26]. There, two different scenarios are considered: first, a Poisson distributed number of grain centres in the observation window (Poisson process), and second, a fixed number of grains (Binomial process). In statistical physics, these two choices are called the grand canonical and the canonical ensemble. The second moments of geometric quantities show a similar behaviour as thermodynamical quantities in statistical physics [26, 25]. For the perfectly isotropic examples of overlapping discs or spheres, the covariances of the Minkowski functionals are also discussed in [4] or [18], respectively.

This paper is organized in the following way. After introducing Boolean models and geometric functionals in Section 2, Section 3 is devoted to the covariance structure of geometric functionals of Boolean models. First, we present general covariance formulae. Then, we concentrate on planar Boolean models. Univariate and

multivariate central limit theorems for geometric functionals of Boolean models are discussed in Section 4. In Section 5, we explicitly compute the covariance formulae for a special Boolean model of aligned rectangles. In the final Section 6, we present and discuss simulation results for Boolean models with rectangles and compare them with our theoretical findings. The agreement is excellent.

Let us finish this introduction with an informal summary of our results for applied scientists. We calculate for certain models of disordered systems of overlapping grains the second moments of a quite general class of robust shape descriptors, which include as well-known examples volume, surface area, Euler characteristic, and, more generally, all Minkowski functionals and tensors. Our results apply to general anisotropic grain distributions, see Theorems 2 and 3. The anisotropic case of aligned (planar) rectangles is discussed in great detail; see Section 5 and Fig. 2. It is interesting to note that the asymptotic formulae for the infinite volume system are actually exact for finite systems with periodic boundary conditions; see Subsection 3.3. The central limit theorem for the geometric functionals (see Theorems 5 and 6) ascertains that in the limit of infinite system size the probability distributions of the normalized geometric functionals are normal distributions. If the structure of a given sample is reasonably well described by the (joint) cumulative probability distributions of the geometric functionals, it is possible to construct tests of certain model hypotheses for random heterogeneous media based on the asymptotic normality and our explicit covariance formulae. We discuss the behaviour of the second moments (e.g., how they differ for various models) and probability distributions in finite systems for specific examples: either aligned or isotropically oriented rectangles (distributed randomly in space). Moreover, we derive explicit formulae (see Fig. 2) and compare the results to simulations (see Figs. 3 and 5).

2 Preliminaries

In the introduction we have defined a Boolean model in terms of a stationary Poisson process in $\mathbb{R}^n$ which is independently marked with random convex bodies, see, e.g., [14]. In this paper we use an equivalent description based on a Poisson process in the space $\mathscr{K}^n$ of convex bodies. For our purposes this representation is more convenient.

We equip $\mathscr{K}^n$ with its Borel σ-field $\mathscr{B}(\mathscr{K}^n)$ with respect to the Hausdorff metric. We call a measure Θ on $\mathscr{K}^n$ locally finite if

$$\Theta(\{K \in \mathscr{K}^n : K \cap C \neq \emptyset\}) < \infty, \quad C \in \mathscr{C}^n,$$

where $\mathscr{C}^n$ is the space of compact subsets of $\mathbb{R}^n$. Let $\mathbf{N}$ be the space of all locally finite counting measures on $\mathscr{K}^n$ and let it be equipped with the smallest σ-field $\mathscr{N}$ such that all maps $\nu \mapsto \nu(A)$, $A \in \mathscr{B}(\mathscr{K}^n)$, from $\mathbf{N}$ to $\mathbb{N} \cup \{0, \infty\}$ are measurable. Each element $\nu \in \mathbf{N}$ has a representation

$$\nu = \sum_{i=1}^{N} \delta_{K_i}, \quad K_1, K_2, \ldots \in \mathscr{K}^n, \quad N \in \mathbb{N} \cup \{0, \infty\},$$

where δ_K stands for the Dirac measure concentrated at $K \in \mathscr{K}^n$. Because of this representation one can think of ν as a countable collection of convex bodies (or grains).

Throughout this paper all random objects are defined on a fixed (sufficiently rich) probability space $(\Omega, \mathscr{A}, \mathbf{P})$. We call a random element η in $\mathbf{N}$ a Poisson process with a locally finite intensity measure Θ if

(i) $\eta(A_1), \ldots, \eta(A_m)$ are independent for disjoint sets $A_1, \ldots, A_m \in \mathscr{B}(\mathscr{K}^n)$,
(ii) $\eta(A)$ follows a Poisson distribution with parameter $\Theta(A)$ for $A \in \mathscr{B}(\mathscr{K}^n)$, i.e.

$$\mathbf{P}(\eta(A) = k) = \frac{\Theta(A)^k}{k!} e^{-\Theta(A)}, \quad k \in \mathbb{N} \cup \{0\}.$$

The second property explains the name. Since $\Theta(A) = \mathbf{E}\eta(A)$ for any $A \in \mathscr{B}(\mathscr{K}^n)$, Θ is called intensity measure of η. The Poisson process η is called stationary if it is invariant under the shifts $K \mapsto K + x := \{y + x : y \in K\}$ for all $x \in \mathbb{R}^n$. This means that the distribution of η does not change under simultaneous translations of its grains. The stationarity of the Poisson process η is equivalent to the translation invariance of the intensity measure Θ.

In the following we always assume that η is a stationary Poisson process in $\mathscr{K}^n$ with an intensity measure Θ such that $\Theta(\mathscr{K}^n) > 0$. It follows from [39, Theorem 4.1.1] that the intensity measure Θ has the representation

$$\Theta(\cdot) = \gamma \iint \mathbf{1}\{K + x \in \cdot\} \, dx \mathbf{Q}(dK),$$

where $\gamma \in (0, \infty)$ is an intensity parameter and $\mathbf{Q}$ is a probability measure on $\mathscr{K}^n$ such that

$$\int V_n(K + C) \, \mathbf{Q}(dK) < \infty, \quad C \in \mathscr{C}^n. \tag{1}$$

Without loss of generality we can assume in the following that $\mathbf{Q}$ is concentrated on the convex bodies with the centre of the circumscribed ball as origin. A random convex body Z_0 distributed according to the probability measure $\mathbf{Q}$ is called typical grain. It follows from Steiner's formula that (1) is equivalent to

$$v_i := \mathbf{E}V_i(Z_0) < \infty, \quad i = 0, \ldots, n,$$

where $V_0, \ldots, V_n$ stand for the intrinsic volumes. Later we shall require that some higher moments of the intrinsice volumes exist. When studying covariances we have to assume that

$$\mathbf{E}V_i(Z_0)^2 < \infty, \quad i = 0, \ldots, n. \tag{2}$$

For some results we need the stronger assumption that

$$\mathbf{E}V_i(Z_0)^3 < \infty, \quad i = 0, \ldots, n. \tag{3}$$

The Boolean model Z based on the Poisson process η is the union of all grains of the Poisson process η, that is

$$Z := \bigcup_{K\in\eta} K.$$

This is a random closed set, whose distribution is completely determined by the intensity γ and the distribution of the typical grain Z_0. The stationarity of the Poisson process η implies the stationarity of the Boolean model Z, that is, the distribution of Z is invariant under translations. Throughout this paper we investigate the stationary Boolean model Z within compact convex observation windows. For a convex body $W \in \mathscr{K}^n$ the number of convex bodies of η that intersect W is almost surely finite so that the random closed set $Z \cap W$ belongs almost surely to the convex ring $\mathscr{R}^n$, which is the set of all unions of finitely many convex bodies and the empty set. Most results in this paper are for the asymptotic regime that the observation window is increased. More precisely, we shall assume that the inradius of the observation window goes to infinity.

To study the behaviour of the intersection of the Boolean model with the observation window W, we consider functionals of $Z \cap W$ with specific properties. We say that a functional $\psi : \mathscr{R}^n \to \mathbb{R}$ is

(i) additive, if $\psi(\emptyset) = 0$, and $\psi(A\cup B) = \psi(A) + \psi(B) - \psi(A\cap B)$ for all $A, B \in \mathscr{R}^n$;
(ii) locally bounded, if

$$M(\psi) := \sup\{|\psi(K+x)| : x \in \mathbb{R}^n, K \in \mathscr{K}^n \text{ with } K \subset [0,1]^n\} < \infty;$$

(iii) translation invariant, if $\psi(A+x) = \psi(A)$, for any $A \in \mathscr{R}^n$ and any $x \in \mathbb{R}^n$.

A measurable functional $\psi : \mathscr{R}^n \to \mathbb{R}$ with all three properties is called geometric. In this case property (ii) can be simplified using the translation invariance (iii). Simple examples of geometric functionals are volume and surface area. These functionals are generalized by the intrinsic volumes $V_0, \dots, V_n$, where V_n is the volume, V_{n-1} is half the surface area (if the set is the closure of its interior) and V_0 is the Euler characteristic.

More general geometric functionals are of the form

$$V_{g,i}(A) := \Psi_i(A; g) := \int g(u)\, \Psi_i(A; du), \quad A \in \mathscr{R}^n, \tag{4}$$

where $\Psi_i(A;\cdot) := \Lambda_i(A; \mathbb{R}^n \times \cdot)$, $i \in \{0,\dots,n\}$, is the (additive extension of the) i-th area measure of A (a measure on the unit sphere $\mathbb{S}^{n-1}$ in $\mathbb{R}^n$), and $g : \mathbb{S}^{n-1} \to \mathbb{R}$ is measurable and bounded. If $g \equiv 1$, then $V_{g,i} = V_i$. We refer to [37, p. 216] for more detail on the support measures Λ_i. An example for geometric functionals of the form (4) are the so-called harmonic intrinsic volumes, which are used in [12] to give a representation of the intensity γ of non-isotropic Boolean models.

The next class of geometric functionals we consider are the components of translation invariant Minkowski tensors (see [38, 17] for a more detailed introduction to

tensor valuations). Let us denote by $\mathbb{T}^s$ the space of s-dimensional tensors in $\mathbb{R}^n$. Let $(e_1,\dots,e_n)$ denote the standard basis of $\mathbb{R}^n$. Then, for $u\in\mathbb{R}^n$ and $s\in\mathbb{N}$, the s-dimensional tensor u^s is given by its coordinates

$$(u^s)_{i_1,\dots,i_s}=\prod_{j=1}^{s}u_{i_j},\quad i_1,\dots,i_s\in\{1,\dots,n\}$$

with respect to the tensor basis $e_{j_1}\otimes\cdots\otimes e_{j_s}$, $j_1,\dots,j_s\in\{1,\dots,n\}$. See [17] for a description in terms of a basis of the vector space $\mathbb{T}^s$ of symmetric tensors.

Now the Minkowski tensors $\Phi_m^{0,s}:\mathscr{R}^n\to\mathbb{T}^s$, $s\in\mathbb{N}$, $m\in\{0,\dots,n-1\}$, are given by

$$\Phi_m^{0,s}(A)=\frac{1}{s!}\frac{\omega_{d-m}}{\omega_{d-m+s}}\int u^s\,\Psi_m(A;du),$$

where $\omega_i:=i\kappa_i$ with κ_i being the volume of the unit ball in $\mathbb{R}^i$. Each component of $\Phi_m^{0,s}$ is obviously measurable, additive and translation invariant. For any $i_1,\dots,i_r\in\{1,\dots,n\}$ and $u\in\mathbb{S}^{n-1}$ we have $|(u^r)_{i_1,\dots,i_r}|\le 1$ so that

$$|(\Phi_m^{0,s}(K))_{i_1,\dots,i_r}|\le\frac{1}{s!}\frac{\omega_{d-m}}{\omega_{d-m+s}}\int 1\,\Psi_m(K;du)=\frac{1}{s!}\frac{\omega_{d-m}}{\omega_{d-m+s}}V_m(K)$$

for $K\in\mathscr{K}^n$. This shows that the components are also locally bounded.

3 Covariance structure

We first consider general covariance formulae for geometric functionals of Boolean models in any dimension n. Then, we concentrate on planar Boolean models and derive explicit integral formulae for the asymptotic covariances of intrinsic volumes.

3.1 General covariance formulae

In this subsection we consider the asymptotic covariance of two geometric functionals of the Boolean model Z within an observation window W as the inradius of W is increased. This means that we consider sequences of convex bodies $(W_i)_{i\in\mathbb{N}}$ such that $r(W_i)\to\infty$ as $i\to\infty$, where $r(K)$ stands for the inradius of a convex body $K\in\mathscr{K}^n$. We denote this asymptotic regime by $r(W)\to\infty$ in the sequel.

In order to present a formula for the asymptotic covariance of two geometric functionals of a Boolean model Z we have to introduce some notation. For a geometric functional $\psi:\mathscr{R}^n\to\mathbb{R}$ the integrability assumption (1) implies for any $A\in\mathscr{R}^n$ that $\mathbf{E}|\psi(Z\cap A)|<\infty$; see [16]. Hence we can define $\psi^*:\mathscr{R}^n\to\mathbb{R}$ by

$$\psi^*(A)=\mathbf{E}\psi(Z\cap A)-\psi(A),\quad A\in\mathscr{R}^n.$$

The functional ψ^* is again geometric, see [16, (3.11)]. The mapping $\psi \mapsto \psi^*$ is a key operation for the second order analysis of the Boolean model. The following proposition provides explicit formulae in some important examples. To state these (and other formulae) we need the measure $\overline{\Psi}_{n-1}(\cdot) := \mathbf{E}\Psi_{n-1}(Z_0;\cdot)$. For a bounded measurable function $g : \mathbb{S}^{n-1} \to \mathbb{R}$ we use the notation

$$\overline{\Psi}_{n-1}(g) := \int g(u)\,\overline{\Psi}_{n-1}(du) = \mathbf{E}\int g(u)\,\Psi_{n-1}(Z_0;du).$$

The *volume fraction* of Z is defined by $p := \mathbf{E}V_n(Z\cap[0,1]^n)$ and can be expressed in the form

$$p = 1 - e^{-\gamma v_n}. \tag{5}$$

Proposition 1. *Let $g : \mathbb{S}^{n-1} \to \mathbb{R}$ be bounded and measurable. Then*

$$V_n^* = -(1-p)V_n, \tag{6}$$

$$V_{g,n-1}^* = -(1-p)V_{g,n-1} + (1-p)\gamma\overline{\Psi}_{n-1}(g)V_n. \tag{7}$$

Proof. Formula (6) follows from an easy calculation; see [16]. For $j \in \{0,\dots,n-1\}$ and $K_0 \in \mathscr{K}$ we obtain from Theorem 9.1.2 in [39] that

$$\mathbf{E}V_{g,j}(Z\cap K_0) = \sum_{k=1}^{\infty}\frac{(-1)^{k-1}}{k!}\int \Psi_j(K_0\cap\ldots\cap K_k;g)\,\Theta^k(d(K_1,\dots,K_k)).$$

Using a result in [15, Sections 3.2–3.4] or [13, Theorem 3.1] (for $g\equiv 1$ see also [39, p. 390]), we obtain that

$$\begin{aligned}\mathbf{E}V_{g,j}(Z\cap K_0) = &\sum_{k=1}^{\infty}\frac{(-1)^{k-1}\gamma^k}{k!} \\ &\times \sum_{\substack{m_0,\dots,m_k=j\\ m_0+\ldots+m_k=kn+j}}^{n}\int V^{(j)}_{m_0,\dots,m_k}(K_0,\dots,K_k;g)\,\mathbf{Q}^k(d(K_1,\dots,K_k)),\end{aligned} \tag{8}$$

where

$$V^{(j)}_{m_0,\dots,m_k}(K_0,\dots,K_k;\cdot) := \Lambda^{(j)}_{m_0,\dots,m_k}(K_0,\dots,K_k;(\mathbb{R}^n)^{k+1}\times\cdot)$$

are finite Borel measures on $\mathbb{S}^{n-1}$, the mixed area measures of order j.

Consider (8) for $j = n-1$. In the summation on the right-hand side we have $m_i = n-1$ for exactly one $i \in \{0,\dots,k\}$ and $m_r = n$ for $r \neq i$. Using the decomposability

$$V^{(n-1)}_{n-1,n,\dots,n}(K_0,\dots,K_k;g) = \Psi_{n-1}(K_0;g)V_n(K_1)\cdots V_n(K_k) \tag{9}$$

and the symmetry properties of the mixed area measures (see [15, 13]) we hence obtain that

$$\begin{aligned}&\mathbf{E}V_{g,n-1}(Z\cap K_0)\\&\quad=\Psi_{n-1}(K_0;g)\sum_{k=1}^{\infty}\frac{(-1)^{k-1}\gamma^k}{k!}v_n^k+V_n(K_0)\sum_{k=1}^{\infty}\frac{(-1)^{k-1}\gamma^k}{k!}kv_n^{k-1}\overline{\Psi}_{n-1}(g)\\&\quad=(1-e^{-\gamma v_n})\Psi_{g,n-1}(K_0)+\gamma\overline{\Psi}_{n-1}(g)e^{-\gamma v_n}V_n(K_0).\end{aligned}$$

Inserting here (5) yields formula (7). □

For two geometric functionals ψ,ϕ, we define the inner product

$$\begin{aligned}\rho(\psi,\phi):=\sum_{i=1}^{\infty}\frac{\gamma}{i!}\int_{\mathscr{K}^n}\int_{(\mathscr{K}^n)^{i-1}}&\psi(K_1\cap\ldots\cap K_i)\\&\times\phi(K_1\cap\ldots\cap K_i)\,\Theta^{i-1}(d(K_2,\ldots,K_i))\,\mathbf{Q}(dK_1),\end{aligned}\tag{10}$$

whenever this infinite series is well defined. The importance of this operation for the covariance analysis of the Boolean model is due to Equation (17) below. In Proposition 2 below and in Section 3.2 we shall see that (10) can be computed in some specific examples.

We need to introduce further notation. The mean covariogram of the typical grain Z_0 is

$$C_n(x)=\mathbf{E}V_n(Z_0\cap(Z_0+x)),\quad x\in\mathbb{R}^n.$$

For a measurable and bounded function $g:\mathbb{S}^{n-1}\to\mathbb{R}$ we define

$$C_{n-1}(x;g)=\mathbf{E}\int\mathbf{1}\{y\in Z_0^\circ+x\}g(u)\,\Lambda_{n-1}(Z_0;d(y,u)),\quad x\in\mathbb{R}^n,\tag{11}$$

where A° denotes the interior of A. Moreover, we use the mixed moment measures

$$N_{n-1,n}(\cdot)=\mathbf{E}\iint\mathbf{1}\{(y,u,z)\in\cdot\}\mathbf{1}\{z\in Z_0\}\,\Lambda_{n-1}(Z_0;d(y,u))\,dz$$

and

$$N_{n-1,n-1}(\cdot)=\mathbf{E}\iint\mathbf{1}\{(y,u,z,v)\in\cdot\}\,\Lambda_{n-1}(Z_0;d(y,u))\,\Lambda_{n-1}(Z_0;d(z,v)).$$

Proposition 2. *Let $g,h:\mathbb{S}^{n-1}\to\mathbb{R}$ be bounded and measurable. Then*

$$\rho(V_n,V_n)=\int\left(e^{\gamma C_n(x)}-1\right)dx,\tag{12}$$

$$\rho(V_{g,n-1},V_n)=\gamma\int g(u)e^{\gamma C_n(y-z)}\,N_{n-1,n}(d(y,u,z)),\tag{13}$$

$$\rho(V_0,V_n)=(1-p)^{-1}-1.\tag{14}$$

If, additionally, $\mathbf{P}(V_n(Z_0)>0)=1$, then

$$\rho(V_{g,n-1},V_{h,n-1}) = \gamma^2 \int e^{\gamma C_n(y-z)} C_{n-1}(y-z;g)h(v)\,N_{n-1,n}(d(z,v,y)) + \gamma \int e^{\gamma C_n(y-z)} g(u)h(v)\,N_{n-1,n-1}(d(y,u,z,v)), \quad (15)$$

$$\rho(V_0,V_{g,n-1}) = \gamma(1-p)^{-1}\overline{\Psi}_{n-1}(g). \quad (16)$$

Proof. Formulae (12) and (14) are implied by [16, Theorem 5.2]. The formulae (13) and (16) can be derived as in the proof of the latter theorem; cf. the computation of $\rho_{d-1,d}$ and of $\rho_{0,d}$ in [16].

As in the computation of $\rho_{i,j}$ in [16] (for $i=j=n-1$) we obtain that

$$\rho(V_{g,n-1},V_{h,n-1}) = A_0 + A_1,$$

where

$$A_0 := \gamma^2 \iiiint e^{\gamma C_n(y-z)} \mathbf{1}\{y\in K_2^0, z\in K_1^0\} g(u)h(v) \times \Lambda_{n-1}(K_1;d(y,u))\,\Lambda_{n-1}(K_2;d(z,v))\,\Theta(dK_1)\,\mathbf{Q}(dK_2)$$

and

$$A_1 := \gamma \iiint e^{\gamma C_n(y-z)} g(u)h(v)\,\Lambda_{n-1}(K;d(y,u))\,\Lambda_{n-1}(K;d(z,v))\,\mathbf{Q}(dK).$$

An easy calculation based on the covariance property of Λ_{n-1} shows that

$$A_0 = \gamma^2 \int e^{\gamma C_n(x-z)} C_{n-1}(x-z;g)h(v)\,N_{n-1,n}(d(z,v,x)).$$

As the number A_1 can be expressed directly as an integral with respect to $N_{n-1,n-1}$, (15) follows. □

The following theorem establishes the existence of asymptotic covariances for general geometric functionals. Moreover, formula (17) provides a tool for their computation.

Theorem 1. *Assume that* (2) *is satisfied and let ψ and ϕ be geometric functionals. Then the limit*

$$\sigma(\psi,\phi) := \lim_{r(W)\to\infty} \frac{\mathbf{cov}(\psi(Z\cap W),\phi(Z\cap W))}{V_n(W)}$$

exists and is given by

$$\sigma(\psi,\phi) = \rho(\psi^*,\phi^*). \quad (17)$$

If (3) *holds, there is a constant c_Θ, depending only on Θ, such that, for $W\in\mathscr{K}^n$ with $r(W)\geq 1$,*

$$\left|\frac{\mathbf{cov}(\psi(Z\cap W),\phi(Z\cap W))}{V_n(W)}-\sigma(\psi,\phi)\right|\le\frac{c_\Theta M(\psi)M(\phi)}{r(W)}. \tag{18}$$

Theorem 1 is taken from [16, Theorem 3.1]. Its proof is involved and depends on the Fock space representation [21] and several non-trivial integral-geometric inequalities for geometric functionals. The inequality (18) allows us to control the error if we approximate the exact covariance for a given observation window by the asymptotic covariance. By evaluating the left-hand side of (18) for the volume one obtains a lower bound of order $1/r(W)$ (see [16, Proposition 3.8]), which shows that the rate on the right-hand side of (18) is optimal, in general.

Using Propositions 1 and 2 in formula (17), we obtain the following result for the asymptotic covariances involving volume and surface content.

Theorem 2. *Assume that* (2) *holds and let* $g,h:\mathbb{S}^{n-1}\to\mathbb{R}$ *be measurable and bounded. Then,*

$$\begin{aligned}\sigma(V_n,V_n)&=(1-p)^2\int(e^{\gamma C_n(x)}-1)\,dx,\\ \sigma(V_{g,n-1},V_n)&=-(1-p)^2\gamma\overline{\Psi}_{n-1}(g)\int(e^{\gamma C_n(x)}-1)\,dx\\ &\quad+(1-p)^2\gamma\int g(u)e^{\gamma C_n(x-y)}N_{n-1,n}(d(x,u,y)).\end{aligned}$$

If, in addition, $\mathbf{P}(V_n(Z_0)>0)=1$*, then*

$$\begin{aligned}\sigma(V_{g,n-1},V_{h,n-1})&=(1-p)^2\gamma^2\overline{\Psi}_{n-1}(g)\overline{\Psi}_{n-1}(h)\int(e^{\gamma C_n(x)}-1)\,dx\\ &+(1-p)^2\gamma^2\int e^{\gamma C_n(x-y)}h(u)C_{n-1}(x-y;g)\,N_{n-1,n}(d(y,u,x))\\ &-(1-p)^2\gamma^2\int e^{\gamma C_n(x-y)}\big(g(u)\overline{\Psi}_{n-1}(h)+h(u)\overline{\Psi}_{n-1}(g)\big)\,N_{n-1,n}(d(y,u,x))\\ &+(1-p)^2\gamma\int e^{\gamma C_n(x-y)}g(u)h(v)\,N_{n-1,n-1}(d(x,u,y,v)).\end{aligned}$$

In the case $h=g\equiv 1$ the formula for $\sigma(V_{g,n-1},V_{h,n-1})$ simplifies to [16, Corollary 6.2], that is

$$\begin{aligned}\sigma(V_{n-1},V_{n-1})&=(1-p)^2\gamma^2v_{n-1}^2\int(e^{\gamma C_n(x)}-1)\,dx\\ &\quad+(1-p)^2\gamma^2\int e^{\gamma C_n(x-y)}(C_{n-1}(x-y)-2v_1)\,N_{n-1,n}(d(y,u,x))\\ &\quad+(1-p)^2\gamma\int e^{\gamma C_n(x-y)}\,N_{n-1,n-1}(d(x,u,y,v)),\end{aligned} \tag{19}$$

where $C_{n-1}(x):=C_{n-1}(x;1)$ is defined by Eq. (11) with $g\equiv 1$.

In the planar case (treated in Subsection 3.2) we will complement Theorem 2 with the asymptotic covariances involving the Euler characteristic. Integral representations of asymptotic covariances of intrinsic volumes in general dimensions

(with respect to some special curvature based measures) can be found in [16, Sections 5 and 6].

Theorem 1 establishes the existence of an asymptotic covariance matrix $\Sigma = (\sigma(\psi_i,\psi_j))_{i,j=1,\dots,m}$ for geometric functionals $\psi_1,\dots,\psi_m$. It is natural to ask whether this matrix is positive definite. The next result (see [16, Theorem 4.1]) gives sufficient, but presumably not necessary conditions for positive definiteness.

Theorem 3. *Let* (2) *be satisfied and assume that* $\mathbf{P}(V_n(Z_0)>0)>0$. *Let* $\psi_0,\dots,\psi_n$ *be geometric functionals such that, for* $i\in\{0,\dots,n\}$, ψ_i *is homogeneous of degree* i *(that is,* $\psi_i(\lambda K)=\lambda^i\psi_i(K)$ *for* $\lambda>0$*) and satisfies*

$$|\psi_i(K)|\geq\tilde{\beta}(\psi_i)r(K)^i,\quad K\in\mathscr{K}^n,$$

with a constant $\tilde{\beta}(\psi_i)$ *only depending on* ψ_i. *Then* $\Sigma=(\sigma(\psi_i,\psi_j))_{0\leq i,j\leq n}$ *is positive definite.*

Since the intrinsic volumes satisfy the assumptions of Theorem 3, we obtain the following corollary.

Corollary 1. *Let* (2) *be satisfied and assume that the typical grain has nonempty interior with positive probability. Then the matrix* $\Sigma=(\sigma(V_i,V_j))_{i,j=0,\dots,n}$ *is positive definite.*

3.2 Covariance formulae for planar Boolean models

In this section we consider the Boolean model in the planar case $n=2$. For measurable and bounded $g:\mathbb{S}^1\to\mathbb{R}$ we consider the additive and measurable functional

$$V_{g,1}(K):=\Psi_1(K;g):=\int g(u)\,\Psi_1(K;du),\quad K\in\mathscr{R}^n,$$

see (4). We will compute the asymptotic covariances between V_0 and the vector $(V_0,V_{g,1},V_2)$.

We define a function $\bar{h}:\mathbb{S}^1\to\mathbb{R}$ by

$$\bar{h}(u):=\int h(K^*,u)\,\mathbf{Q}(dK),\quad u\in\mathbb{S}^1,$$

where $K^*:=-K$ and $h(K^*,\cdot)$ is the support function of K^*. Indeed, if K is a convex body containing the origin, then the basic properties of V_1 together with the definition of the support function easily imply that $0\leq h(K^*,u)\leq cV_1(K^*)=cV_1(K)$ for a constant $c>0$ that does only depend on the dimension. Therefore dominated convergence implies that $\bar{h}$ is continuous and in particular bounded. We also define

$$v_{1,1}:=\overline{\Psi}_1(\bar{h})=\int\bar{h}(u)\,\overline{\Psi}_1(du)=\iiint h(K^*,u)\,\overline{\Psi}_1(L;du)\,\mathbf{Q}(dK)\,\mathbf{Q}(dL).$$

Theorem 4. *Assume that* (2) *and* $\mathbf{P}(V_2(Z_0) > 0) = 1$ *hold and let* $g : \mathbb{S}^1 \to \mathbb{R}$ *be measurable and bounded. Then*

$$\begin{aligned}
\sigma(V_0, V_2) &= p(1-p) - (1-p)^2\gamma(1-\gamma\nu_{1,1}) \int \left(e^{\gamma C_2(x)} - 1\right) dx \\
&\quad - 2(1-p)^2\gamma^2 \int \overline{h}(u) e^{\gamma C_2(y-z)} N_{1,2}(d(y,u,z)), \qquad (20) \\
\sigma(V_0, V_{g,1}) &= (1-p)^2\gamma\overline{\Psi}_1(g) + (1-p)^2\gamma^2\overline{\Psi}_1(g)(1-\gamma\nu_{1,1}) \int \left(e^{\gamma C_2(x)} - 1\right) dx \\
&\quad + (1-p)^2 \int \left(\chi'(y-z)g(u) + 2\gamma^3\overline{\Psi}_1(g) e^{\gamma C_2(y-z)} \overline{h}(u)\right) N_{1,2}(d(z,u,y)) \\
&\quad - 2(1-p)^2\gamma^2 \int e^{\gamma C_2(y-z)} \overline{h}(u) g(v) N_{1,1}(d(y,u,z,v)), \qquad (21) \\
\sigma(V_0, V_0) &= (1-2p)(1-p)\gamma + (1-p)(2p-3)\nu_{1,1}\gamma^2 \\
&\quad + (1-p)^2\gamma^2(1-\gamma\nu_{1,1})^2 \int \left(e^{\gamma C_2(x)} - 1\right) dx \\
&\quad + (1-p)^2 \int \overline{h}(u) \chi''(y-z) N_{1,2}(d(z,u,y)) \\
&\quad + 4(1-p)^2\gamma^3 \int e^{\gamma C_2(y-z)} \overline{h}(u) \overline{h}(v) N_{1,1}(d(y,u,z,v)), \qquad (22)
\end{aligned}$$

where

$$\begin{aligned}
\chi'(x) &:= e^{\gamma C_2(x)} \left(\gamma^3(\nu_{1,1} - 2C_1(x;\overline{h})) - \gamma^2\right), \quad x \in \mathbb{R}^2, \\
\chi''(x) &:= e^{\gamma C_2(x)} \left(4\gamma^4(C_1(x;\overline{h}) - \nu_{1,1}) + 4\gamma^3\right), \quad x \in \mathbb{R}^2.
\end{aligned}$$

Proof. We wish to apply (17). In view of Proposition 1 we need to determine V_0^*. To do so we consider (8) for $j = 0$ and $g \equiv 1$. For the summation we distinguish four cases. In the first two cases we have $m_i = 0$ for exactly one $i \in \{0, \dots, k\}$ and either $m_0 = 0$ or $m_0 = 2$. In the third and fourth case we have $m_i = m_r = 1$ for exactly two $i, r \in \{0, \dots, k\}$ and either $m_0 = 0$ or $m_0 = 1$. Accordingly we can write

$$\mathbf{E}V_0(Z \cap K_0) = \sum_{k=1}^{\infty} \frac{(-1)^{k-1}\gamma^k}{k!}(a_{1,k} + a_{2,k} + a_{3,k} + a_{4,k}).$$

The decomposability property (9) (for $n = 2$) and the symmetry of mixed functionals imply that

$$a_{1,k} = V_0(K_0)v_2^k, \quad a_{2,k} = V_2(K_0)kv_2^{k-1}.$$

To treat $a_{3,k}$ and $a_{4,k}$ we use the decomposability property

$$V^{(0)}_{1,1,2\dots,2}(K_0, \dots, K_k) = V^{(0)}_{1,1}(K_0, K_1)V_2(K_2) \cdots V_2(K_k)$$

and again the symmetry of mixed functionals (see [15]) to obtain that

$$a_{3,k} = kv_2^{k-1} \int V_{1,1}^{(0)}(K_0,K)\,\mathbf{Q}(dK),$$
$$a_{4,k} = \frac{k(k-1)}{2} v_2^{k-2} V_2(K_0) \int V_{1,1}^{(0)}(K,L)\,\mathbf{Q}^2(d(K,L)).$$

It follows that

$$\begin{aligned} V_0^*(K_0) = & -(1-p)V_0(K_0) + (1-p)\gamma \int V_{1,1}^{(0)}(K_0,K)\,\mathbf{Q}(dK) \\ & + (1-p)V_2(K_0)\left(\gamma - \frac{\gamma^2}{2}\int V_{1,1}^{(0)}(K,L)\,\mathbf{Q}^2(d(K,L))\right) \end{aligned}$$

or

$$\begin{aligned} V_0^*(K_0) = & -(1-p)V_0(K_0) + (1-p)\gamma \overline{V}_{1,1}(K_0) \\ & + (1-p)\left(\gamma - \frac{\gamma^2}{2} w_{1,1}\right) V_2(K_0), \end{aligned} \tag{23}$$

where

$$\overline{V}_{1,1}(K_0) := \int V_{1,1}^{(0)}(K_0,K)\,\mathbf{Q}(dK),$$
$$w_{1,1} := \int V_{1,1}^{(0)}(K,L)\,\mathbf{Q}^2(d(K,L)).$$

Using (17) together with (23) and Proposition 1, we obtain the following intermediate formulae for the asymptotic covariances:

$$\begin{aligned} \sigma(V_0,V_2) = & (1-p)^2\rho(V_0,V_2) - (1-p)^2\gamma\rho(\overline{V}_{1,1},V_2) \\ & - (1-p)^2\left(\gamma - \frac{\gamma^2}{2} w_{1,1}\right)\rho(V_2,V_2), \end{aligned} \tag{24}$$

$$\begin{aligned} \sigma(V_0,V_{g,1}) = & -(1-p)^2\gamma\overline{\Psi}_1(g)\rho(V_0,V_2) + (1-p)^2\gamma^2\overline{\Psi}_1(g)\rho(\overline{V}_{1,1},V_2) \\ & + (1-p)^2\overline{\Psi}_1(g)\left(\gamma^2 - \frac{\gamma^3}{2} w_{1,1}\right)\rho(V_2,V_2) \\ & + (1-p)^2\rho(V_0,V_{g,1}) - (1-p)^2\gamma\rho(\overline{V}_{1,1},V_{g,1}) \\ & - (1-p)^2\left(\gamma - \frac{\gamma^2}{2} w_{1,1}\right)\rho(V_2,V_{g,1}), \end{aligned} \tag{25}$$

and

$$\begin{aligned}\sigma(V_0,V_0) &= (1-p)^2\rho(V_0,V_0) - 2(1-p)^2\gamma\rho(V_0,\overline{V}_{1,1})\\ &\quad + (1-p)^2\gamma^2\rho(\overline{V}_{1,1},\overline{V}_{1,1}) - 2(1-p)^2\Big(\gamma-\frac{\gamma^2}{2}w_{1,1}\Big)\rho(V_0,V_2)\\ &\quad + 2(1-p)^2\Big(\gamma^2-\frac{\gamma^3}{2}w_{1,1}\Big)\rho(\overline{V}_{1,1},V_2)\\ &\quad + (1-p)^2\Big(\gamma-\frac{\gamma^2}{2}w_{1,1}\Big)^2\rho(V_2,V_2). \qquad (26)\end{aligned}$$

At this stage we can use the formula

$$V_{1,1}^{(0)}(K,L) = 2\int h(L^*,u)\,\Psi_1(K;du), \quad K,L\in\mathscr{K},$$

(use (6.25) and (14.21) in [39] as well as $S_1 = 2\Psi_1$) implying that

$$\overline{V}_{1,1}(K) = 2\int \bar{h}(u)\,\Psi_1(K;du) = 2V_{\bar{h},1}(K), \qquad (27)$$

$$w_{1,1} = \int \overline{V}_{1,1}(K)\,\mathbf{Q}(dK) = 2\overline{\Psi}_1(\bar{h}) = 2v_{1,1}. \qquad (28)$$

Theorem 5.2 in [16] implies that

$$\rho(V_0,V_0) = e^{\gamma v_2}\Big(\gamma+\frac{\gamma^2 v'_{1,1}}{2}\Big),$$

where

$$v'_{1,1} := \int \Phi_0(K_1\cap(K_2+x);\partial K_1\cap(\partial K_2+x))\,dx\,\mathbf{Q}^2(d(K_1,K_2)).$$

It follows from [39, Theorem 6.4.1] (together with the decomposability property and the fact that the boundary of a convex body has vanishing volume) that

$$\int \Phi_0(K_1\cap(K_2+x);\partial K_1\cap(\partial K_2+x))\,dx = \Phi_{1,1}^{(0)}(K_1,K_2;\partial K_1\times\partial K_2),$$

where $\Phi_{1,1}^{(0)}(K_1,K_2;\cdot)$ is a mixed functional. Since $\Phi_{1,1}^{(0)}(K_1,K_2;\cdot)$ is concentrated on $\partial K_1\times\partial K_2$ by [39, Theorem 6.4.1 (b)], we have

$$\Phi_{1,1}^{(0)}(K_1,K_2;\partial K_1\times\partial K_2) = \Phi_{1,1}^{(0)}(K_1,K_2;\mathbb{R}^2\times\mathbb{R}^2) = V_{1,1}^{(0)}(K_1,K_2).$$

Therefore $v'_{1,1} = w_{1,1} = 2v_{1,1}$ and

$$\rho(V_0,V_0) = (1-p)^{-1}(\gamma+\gamma^2 v_{1,1}). \qquad (29)$$

Now we can insert (27) and (28) as well as (29) and the formulae of Proposition 2 into (24)–(26) to obtain the assertions. From (24) we get

$$\sigma(V_0,V_2) = (1-p)^2\rho(V_0,V_2) - (1-p)^2\gamma 2\rho(V_{\bar{h},1},V_2) - (1-p)^2(\gamma-\gamma^2 v_{1,1})\rho(V_2,V_2)$$

so that (20) follows from (14), (13) and (12).

Next we deduce from (25) that

$$\begin{aligned}\sigma(V_0,V_{g,1}) = {} & -p(1-p)\gamma\overline{\Psi}_1(g) \\ & + 2(1-p)^2\gamma^3\overline{\Psi}_1(g)\int \bar{h}(u)e^{\gamma C_2(y-z)}N_{1,2}(d(y,u,z)) \\ & + (1-p)^2\overline{\Psi}_1(g)(\gamma^2-\gamma^3 v_{1,1})\int \left(e^{\gamma C_2(x)}-1\right)dx \\ & + (1-p)^2\gamma e^{\gamma v_2}\overline{\Psi}_1(g) \\ & - 2(1-p)^2\gamma^3\int e^{\gamma C_2(y-z)}C_1(y-z;\bar{h})g(v)N_{1,2}(d(z,v,y)) \\ & - 2(1-p)^2\gamma^2\int e^{\gamma C_2(y-z)}\bar{h}(u)g(v)N_{1,1}(d(y,u,z,v)) \\ & - (1-p)^2\left(\gamma^2-\gamma^3 v_{1,1}\right)\int g(u)e^{\gamma C_2(y-z)}N_{1,2}(d(y,u,z)).\end{aligned}$$

Equation (21) follows upon some simplification and rearrangement.

From (26) we obtain that

$$\begin{aligned}\sigma(V_0,V_0) = {} & (1-p)\left(\gamma+\gamma^2 v_{1,1}\right) - 4(1-p)\gamma^2 v_{1,1} \\ & + 4(1-p)^2\gamma^4\int e^{\gamma C_2(y-z)}C_1(y-z;\bar{h})\bar{h}(v)N_{1,2}(d(z,v,y)) \\ & + 4(1-p)^2\gamma^3\int e^{\gamma C_2(y-z)}\bar{h}(u)\bar{h}(v)N_{1,1}(d(y,u,z,v)) \\ & - 2(1-p)^2\left(\gamma-\gamma^2 v_{1,1}\right)\left((1-p)^{-1}-1\right) \\ & + 4(1-p)^2(\gamma^3-\gamma^4 v_{1,1})\int \bar{h}(u)e^{\gamma C_2(y-z)}N_{1,2}(d(y,u,z)) \\ & + (1-p)^2\left(\gamma-\gamma^2 v_{1,1}\right)^2\int \left(e^{\gamma C_2(x)}-1\right)dx.\end{aligned}$$

Equation (22) now follows from an easy calculation. □

In the isotropic case, $\bar{h} := \bar{h}(u)$ does not depend on $u \in \mathbb{S}^1$. By [39, (14.21)], we have for $L \in \mathscr{K}^n$

$$V_1(L) = \int h(L,u)\,\Psi_1(B^2;du) = \frac{1}{2}\int h(L,u)\,\mathscr{H}^1(du),$$

so that

$$v_1 = \frac{1}{2}\iint h(L,u)\,\mathscr{H}^1(du)\,\mathbf{Q}(dL) = \pi\bar{h}.$$

Further

$$v_{1,1} = \iint \bar{h}(u)\,\Psi_1(K;du)\,\mathbf{Q}(dK) = \bar{h}v_1.$$

Hence

$$\bar{h} = \frac{v_1}{\pi}, \quad v_{1,1} = \frac{v_1^2}{\pi}. \tag{30}$$

Inserting (30) into (20)–(22) yields Corollary 6.3 in [16].

3.3 The Boolean model on the torus

One obtains the n-dimensional (unit) torus T^n by identifying opposite sides of the boundary of $[-1/2,1/2]^n$. As in $\mathbb{R}^n$ one can consider a translation invariant Poisson process of grains on the torus (with intensity measure Λ, grain distribution $\mathbf{Q}$ and intensity γ) and consider the resulting Boolean model Z_{T^n}. The Boolean model on the torus T^n can be constructed in the following way from a random closed set in $\mathbb{R}^n$ (see Fig. 1). We start with a homogeneous Poisson process in $[-1/2,1/2]^n$ and put around each point an independent copy of the typical grain. For each grain, we also place all translates by vectors $v \in \mathbb{Z}^n$ and take the union of all resulting grains. Finally, we restrict this random closed set to $[-1/2,1/2]^n$ and identify opposite boundaries. This setting is also denoted as periodic boundary conditions.

For a geometric functional $\psi : \mathscr{R}^n \to \mathbb{R}$ we can define $\psi(Z_{T^n})$ in the following way. For a set $K \subset T^n$ whose embedding $K_{\mathbb{R}^n} = \{x \in \mathbb{R}^n : x \in K\}$ into $\mathbb{R}^n$ is a convex body and is contained in $(-1/2,1/2)^n$ we put $\psi(K) = \psi(K_{\mathbb{R}^n})$. By further requiring that ψ is translation-invariant and additive on T^n, this gives us $\psi(Z_{T^n})$.

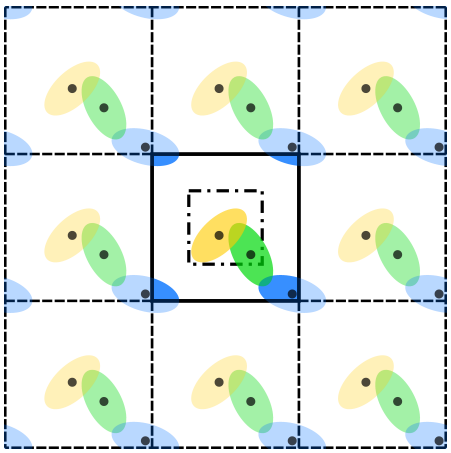

Fig. 1 The Boolean model with periodic boundary conditions: we consider grains with centers in $[-1/2,1/2]^n$ (square with solid line) and all their translations by $\mathbb{Z}^n$ valued vectors (in squares with dashed lines). The Boolean model with periodic boundary conditions is obtained by taking the union of all the grains and restricting to the square with the solid line.

By computing the Fock space representation of $\psi(Z_{T^n})$ and $\phi(Z_{T^n})$ for geometric functionals $\psi,\phi : \mathscr{R}^n \to \mathbb{R}$ as in [16, Section 3] for a Boolean model in $\mathbb{R}^n$, one obtains that

$$\begin{aligned}&\mathbf{cov}(\psi(Z_{T^n}),\phi(Z_{T^n}))\\&= \sum_{n=1}^{\infty} \frac{\gamma}{n!} \iint (\mathbf{E}\psi(Z_{T^n}\cap K_1\cap\ldots\cap K_n) - \psi(K_1\cap\ldots\cap K_n))\\&\qquad \times (\mathbf{E}\phi(Z_{T^n}\cap K_1\cap\ldots\cap K_n) - \phi(K_1\cap\ldots\cap K_n))\,\Lambda^{n-1}(d(K_2,\ldots,K_n))\,\mathbf{Q}(dK_1).\end{aligned}$$

Now let us assume that the grain distribution $\mathbf{Q}$ is such that the typical grain Z_0 is almost surely contained in $[-1/4,1/4]^n$, which is depicted by the dot-dash line in Fig. 1. In this case the intersection of two grains is always convex and the intersections on the right-hand side of the covariance formula are the same as for a Boolean model in $\mathbb{R}^n$ with grain distribution $\mathbf{Q}$ and intensity γ. Thus, it follows from the above definition of ψ and ϕ of a subset of the torus whose embedding into $\mathbb{R}^n$ is a convex body and a subset of $(-1/2,1/2)^n$ and the additivity that

$$\mathbf{cov}(\psi(Z_{T^n}),\phi(Z_{T^n})) = \rho(\psi^*,\phi^*).$$

In other words, if the typical grain is sufficiently bounded, the exact covariances for the Boolean model on the torus coincide with the asymptotic covariances for the corresponding Boolean model in $\mathbb{R}^n$. This provides a way to compute estimates for the asymptotic covariances via simulations on the torus.

4 Central limit theorems

In this section we consider the asymptotic behaviour of the distributions of geometric functionals or of vectors of geometric functionals for growing observation window. Recall that a sequence of m-dimensional random vectors $(Y_i)_{i\in\mathbb{N}}$ converges in distribution to an m-dimensional random vector Y if

$$\lim_{i\to\infty} \mathbf{P}(Y_i \le x) = \mathbf{P}(Y \le x)$$

for all $x \in \mathbb{R}^m$ such that $y \mapsto \mathbf{P}(Y \le y)$ is continuous at x. (Here the relation $\le$ is to be understood componentwise). In this case we write $Y_i \xrightarrow{d} Y$ (as $i \to \infty$). We are not only interested in the convergence in distribution but also in error bounds. In order to measure the distance between the distributions of two m-dimensional random vectors Z_1, Z_2, we use the d_3-metric which is given by

$$d_3(Z_1,Z_2) = \sup_{h\in\mathscr{H}_m} |\mathbf{E}h(Z_1) - \mathbf{E}h(Z_2)|,$$

where $\mathscr{H}_m$ is the set of all C^3-functions $h:\mathbb{R}^m\to\mathbb{R}$ such that the absolute values of the second and the third partial derivatives are bounded by one. For two random variables Z_1,Z_2 we consider the Wasserstein distance

$$d_W(Z_1,Z_2)=\sup_{h\in\mathrm{Lip}(1)}|\mathbf{E}h(Z_1)-\mathbf{E}h(Z_2)|,$$

where $\mathrm{Lip}(1)$ is the set of all functions $h:\mathbb{R}\to\mathbb{R}$ whose Lipschitz constant is at most one. Note that convergence in the d_3-distance or in the Wasserstein distance implies convergence in distribution.

For the quantitative bounds we assume that there is a constant $\varepsilon>0$ such that

$$\mathbf{E}V_i(Z_0)^{3+\varepsilon}<\infty,\quad i=0,\dots,n. \tag{31}$$

We begin with a multivariate central limit theorem for a vector of geometric functionals.

Theorem 5. *Assume that* (2) *is satisfied, let* $\Psi:=(\psi_1,\dots,\psi_m)$ *for geometric functionals* $\psi_1,\dots,\psi_m$*, and let* N_Σ *be an* m*-dimensional centred Gaussian random vector with covariance matrix* $\Sigma=(\sigma(\psi_i,\psi_j))_{i,j=1,\dots,m}$*. Then*

$$\frac{1}{\sqrt{V_n(W)}}\big(\Psi(Z\cap W)-\mathbf{E}\Psi(Z\cap W)\big)\xrightarrow{d}N_\Sigma\quad\text{as}\quad r(W)\to\infty.$$

If (31) *holds, there is a constant* $C_{\psi_1,\dots,\psi_m}$ *depending on* $\psi_1,\dots,\psi_m$*,* Θ *and* ε *such that*

$$d_3\left(\frac{1}{\sqrt{V_n(W)}}\big(\Psi(Z\cap W)-\mathbf{E}\Psi(Z\cap W)\big),N_\Sigma\right)\le\frac{C_{\psi_1,\dots\psi_m}}{r(W)^{\min\{\varepsilon n/2,1\}}}$$

for $W\in\mathscr{K}^n$ *with* $r(W)\ge 1$.

This result was proved in [16, Theorem 9.1] by using the Stein-Malliavin method and a truncation argument.

As tensors can be interpreted as vectors, we can define convergence of tensor valued random elements and their d_3-distance via convergence and d_3-distance for random vectors. Since the components of $\Phi_m^{0,s}$ are geometric functionals, Theorem 5 can be applied to the translation invariant Minkowski tensors.

Corollary 2. *Assume that* (2) *holds, let* $s\in\mathbb{N}$ *and* $m\in\{0,\dots,n-1\}$ *and let* $N_m^{0,s}$ *be a random element in* $\mathbb{T}^s$ *such that each component is a centred Gaussian random variable and*

$$\mathbf{cov}((N)_{i_1,\dots,i_s},(N)_{j_1,\dots,j_s})=\sigma((\Phi_m^{0,s})_{i_1,\dots,i_s},(\Phi_m^{0,s})_{j_1,\dots,j_s})$$

for $i_1,\dots,i_s,j_s,\dots,j_s\in\{1,\dots,n\}$*. Then*

$$\frac{1}{\sqrt{V_n(W)}}(\Phi_m^{0,s}(Z\cap W)-\mathbf{E}\Phi_m^{0,s}(Z\cap W))\xrightarrow{d}N_m^{0,s}\quad\text{as}\quad r(W)\to\infty.$$

If (31) *holds, there is a constant $C_{s,m}$ depending on s, m, Θ and ε such that*

$$d_3\left(\frac{1}{\sqrt{V_n(W)}}(\Phi_m^{0,s}(Z\cap W)-\mathbf{E}\Phi_m^{0,s}(Z\cap W)),N_m^{0,s}\right)\leq\frac{C_{s,m}}{r(W)^{\min\{\varepsilon n/2,1\}}}$$

for $W\in\mathscr{K}^n$ with $r(W)\geq 1$.

In the multivariate case we assume translation invariance of the geometric functionals in order to ensure the existence of an asymptotic covariance matrix. In the univariate case this is not required since one can standardize be dividing by the standard deviation. For this reason, we can drop the assumption of translation invariance in the following univariate central limit theorem, which is taken from [16, Theorem 9.3].

Theorem 6. *Let* (2) *be satisfied, let $\psi:\mathscr{R}^n\to\mathbb{R}$ be measurable, additive and locally bounded, assume that there are constants $r_0\geq 1$ and $\sigma_0>0$ such that*

$$\frac{\mathbf{var}\,\psi(Z\cap W)}{V_n(W)}\geq\sigma_0$$

for $W\in\mathscr{K}^n$ with $r(W)\geq r_0$ and let N be a standard Gaussian random variable. Then

$$\frac{\psi(Z\cap W)-\mathbf{E}\psi(Z\cap W)}{\sqrt{\mathbf{var}\,\psi(Z\cap W)}}\xrightarrow{d}N\quad as\quad r(W)\to\infty.$$

If, additionally, (31) *is satisfied, there is a constant c_ψ depending on ψ, Θ, r_0, σ_0, and ε such that*

$$d_W\left(\frac{\psi(Z\cap W)-\mathbf{E}\psi(Z\cap W)}{\sqrt{\mathbf{var}\,\psi(Z\cap W)}},N\right)\leq\frac{c_\psi}{V_n(W)^{\min\{\varepsilon/2,1/2\}}}$$

for $W\in\mathscr{K}^n$ with $r(W)\geq r_0$.

The results presented in this section generalize previous findings in [2, 3, 10, 11, 24, 33, 36], which only deal with volume, surface area or closely related functionals.

5 Boolean model of aligned rectangles

In this section we assume that $n=2$ and that the typical grain Z_0 is a deterministic rectangle of the form

$$K:=\left[-\frac{a}{2}e_1,\frac{a}{2}e_1\right]+\left[-\frac{b}{2}e_2,\frac{b}{2}e_2\right]=\left[-\frac{a}{2},\frac{a}{2}\right]\times\left[-\frac{b}{2},\frac{b}{2}\right]$$

for some fixed $a,b>0$, where $e_1:=(1,0)$ and $e_2:=(0,1)$. Then $v_2=ab$ and $v_1=a+b$.

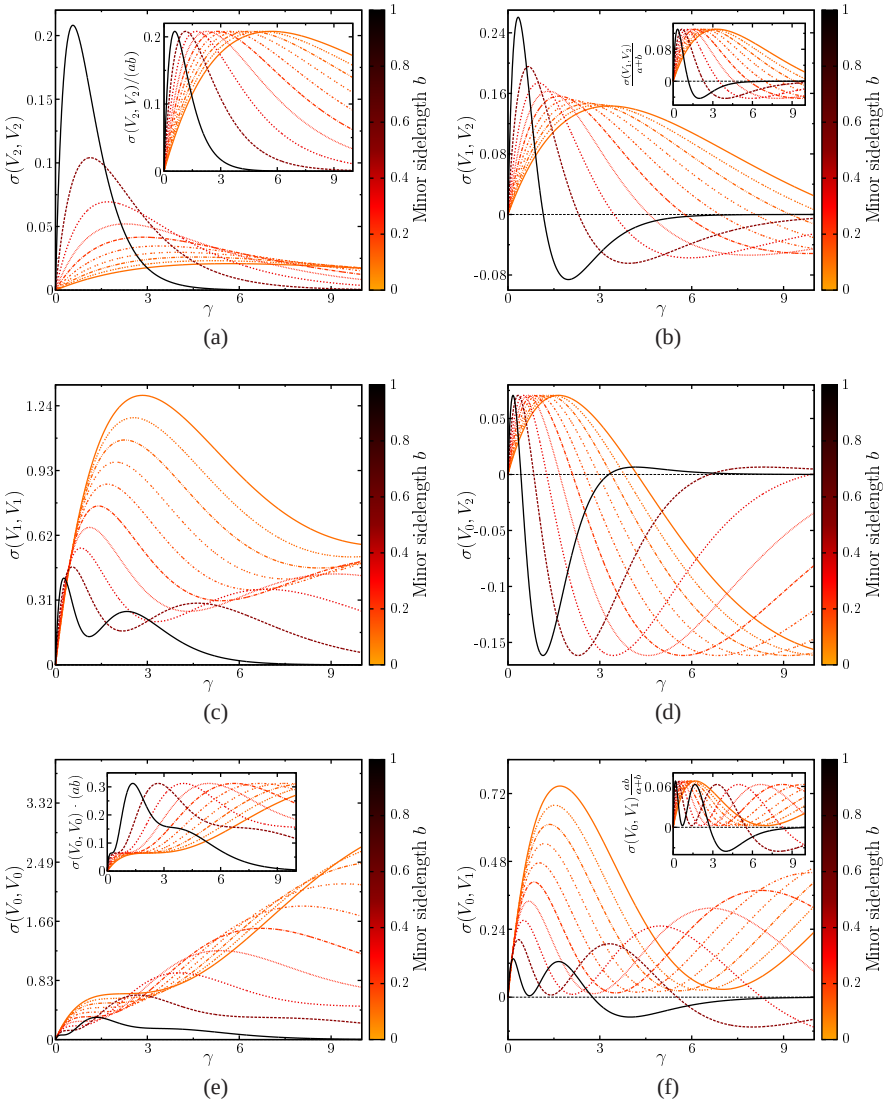

Fig. 2 Asymptotic covariances $\sigma(V_i,V_j)$ as a function of the intensity γ for Boolean models of aligned rectangles with varying aspect ratio b/a; we choose $a=1$, hence $b\in(0,1]$; see Eqs. (34), (42), (44), (52), (55), and (58). The insets show covariances that are rescaled by suitable functions of the side lengths a and b of a single rectangle so that they only depend on $\gamma\nu_2$ but not on the aspect ratio, which also holds for $\sigma(V_0,V_2)$ in (d) without rescaling.

For any $x=(x_1,x_2)\in\mathbb{R}^2$ we have

$$C_2(x)=V_2(K\cap(K+x))=\mathbf{1}\{|x_1|\le a,|x_2|\le b\}(a-|x_1|)(b-|x_2|).$$

A change of variables and a symmetry argument imply that

$$\int \left(e^{\gamma C_2(x)} - 1\right) dx = 4v_2 H(\gamma v_2), \tag{32}$$

where the function $H : [0,\infty) \to [0,\infty)$ is defined by

$$H(r) := \int_0^1 \int_0^1 \left(e^{rst} - 1\right) ds\, dt = \sum_{k=1}^{\infty} \frac{r^k}{k!(k+1)^2}, \quad r \geq 0. \tag{33}$$

Hence we obtain from Theorem 2 that

$$\boxed{\sigma(V_2, V_2) = 4(1-p)^2 v_2 H(\gamma v_2),} \tag{34}$$

where we recall that $p = 1 - e^{-\gamma v_2}$. The variance is visualized in Fig. 2(a).

At this stage it is convenient to complement the definition (33) with the following easy to check formulae:

$$\int_0^1 \int_0^1 e^{rst} s\, ds\, dt = \frac{1}{r^2} e^r - \frac{1}{r^2} - \frac{1}{r}, \tag{35}$$

$$\int_0^1 \int_0^1 e^{rst} s^2\, ds\, dt = \frac{1}{r^2} e^r - \frac{1}{r^3} e^r + \frac{1}{r^3} - \frac{1}{2r}, \tag{36}$$

$$\int_0^1 \int_0^1 e^{rst} st\, ds\, dt = \frac{1}{r^2} e^r - \frac{1}{r^2} - \frac{1}{r} H(r) - \frac{1}{r}. \tag{37}$$

A consequence is

$$\int_0^1 \int_0^1 e^{rst} (st + s^2)\, ds\, dt = \frac{2}{r^2} e^r - \frac{1}{r^3} e^r + \frac{1}{r^3} - \frac{1}{r^2} - \frac{3}{2r} - \frac{1}{r} H(r). \tag{38}$$

Now we use Theorem 2 (for $n = 2$ and $g \equiv 1$) to compute $\sigma(V_1, V_2)$. For any measurable and even functions $f : \mathbb{R}^2 \to [0,\infty)$ and $\tilde{f} : \mathbb{S}^1 \to [0,\infty)$ we have

$$\int f(y-z) \tilde{f}(u)\, N_{1,2}(d(y,u,z)) = a_1^+ + a_1^- + a_2^+ + a_2^-,$$

where

$$a_i^{\pm} := \frac{1}{2} \iint \mathbf{1}\{y \in A_i^{\pm}, z \in K\} f(y-z) \tilde{f}(e_i)\, \mathscr{H}^1(dy)\, dz, \quad i \in \{1,2\}$$

and $A_1^{\pm} := \{(x_1,x_2) \in K : x_1 = \pm a/2\}, A_2^{\pm} := \{(x_1,x_2) \in K : x_2 = \pm b/2\}$. By Fubini and a change of variables

$$a_1^{\pm} = \frac{\tilde{f}(e_1)}{2} \iint \mathbf{1}\{y \in A_1^{\pm}, y+z \in K\} f(z)\, \mathscr{H}^1(dy)\, dz.$$

For any $z = (z_1, z_2) \in K$ with $-a \leq z_1 \leq 0$ and $z_2 \geq 0$ we have

$$\int \mathbf{1}\{y \in A_1, y+z \in K\}\, \mathscr{H}^1(dy) = \mathscr{H}^1([-b/2, b/2 - z_2]) = b - z_2 = b - |z_2|.$$

For $-a \le z_1 \le 0$ and $z_2 \le 0$ this integral takes the same value. Since the set of all z with $z_1 \notin [-a,0]$ or $|z_2| > b$ does not contribute to a^+ while the set of all z with $z_1 \notin [0,a]$ or $|z_2| > b$ does not contribute to a^- it follows that

$$a_1^+ + a_1^- = \frac{\tilde f(e_1)}{2} \int \mathbf{1}\{|z_1| \le a, |z_2| \le b\} f(z_1,z_2)(b - |z_2|)\, d(z_1,z_2).$$

Using a similar result for $b_1^+ + b_1^-$ gives

$$\begin{aligned} &\int f(y-z)\tilde f(u)\, N_{1,2}(d(y,u,z)) \\ &\qquad = \frac{\tilde f(e_1)}{2} \int \mathbf{1}\{|z_1| \le a, |z_2| \le b\} f(z_1,z_2)(b - |z_2|)\, d(z_1,z_2) \\ &\qquad\quad + \frac{\tilde f(e_2)}{2} \int \mathbf{1}\{|z_1| \le a, |z_2| \le b\} f(z_1,z_2)(a - |z_1|)\, d(z_1,z_2). \end{aligned} \tag{39}$$

Inserting here $f(z) := e^{\gamma C_2(z)}$ and using a change of variables gives

$$\begin{aligned} &\int e^{\gamma C_2(y-z)} \tilde f(u)\, N_{1,2}(d(y,u,z)) \\ &\quad = 2ab^2 \tilde f(e_1) \int_0^1 \int_0^1 e^{\gamma a b y_1 y_2} y_2\, dy_1\, dy_2 + 2a^2 b \tilde f(e_2) \int_0^1 \int_0^1 e^{\gamma a b y_1 y_2} y_1\, dy_1\, dy_2. \end{aligned}$$

From (35) we obtain that

$$\begin{aligned} &\int e^{\gamma C_2(y-z)} \tilde f(u)\, N_{1,2}(d(y,u,z)) \\ &\quad = \tilde f(e_1)\left(\frac{2}{\gamma^2 a} e^{\gamma a b} - \frac{2}{\gamma^2 a} - \frac{2b}{\gamma}\right) + \tilde f(e_2)\left(\frac{2}{\gamma^2 b} e^{\gamma a b} - \frac{2}{\gamma^2 b} - \frac{2a}{\gamma}\right). \end{aligned} \tag{40}$$

In the case $\tilde f(e_1) = \tilde f(e_2) = 1$ this yields

$$\int e^{\gamma C_2(x-y)}\, N_{1,2}(d(x,u,y)) = 2v_1\left(\frac{1}{\gamma^2 v_2} e^{\gamma v_2} - \frac{1}{\gamma^2 v_2} - \frac{1}{\gamma}\right). \tag{41}$$

Inserting this result together with (32) into the formula of Theorem 2 yields

$$\boxed{\sigma(V_1,V_2) = 2(1-p)^2 v_1 \left[\frac{1}{\gamma v_2}(e^{\gamma v_2} - 1) - 1 - 2\gamma v_2 H(\gamma v_2)\right],} \tag{42}$$

which is visualized in Fig. 2(b).

Next we use (20) to compute $\sigma(V_0,V_2)$, starting with the observation

$$h(K,-e_1) = h(K,e_1) = \frac{a}{2}, \qquad h(K,-e_2) = h(K,e_2) = \frac{b}{2}.$$

Therefore we obtain from (40)

$$\int \bar{h}(u) e^{\gamma C_2(y-z)} N_{1,2}(d(y,u,z)) = \frac{2}{\gamma^2} e^{\gamma v_2} - \frac{2}{\gamma^2} - \frac{2v_2}{\gamma}. \tag{43}$$

To evaluate

$$v_{1,1} = \int h(K,u)\, \Psi_1(K;du)$$

we split the integration according to $u \in \{-e_1, e_1, -e_2, e_2\}$. As all four integrals yield the same value $ab/4$, we get $v_{1,1} = v_2$. Summarizing, we obtain from (20)

$$\begin{aligned}\sigma(V_0,V_2) = p(1-p) - 4(1-p)^2 \gamma v_2 (1 - 1\gamma v_2) H(\gamma v_2) \\ - 4(1-p)^2 \big((1-p)^{-1} - 1 - \gamma v_2\big),\end{aligned}$$

that is

$$\boxed{\sigma(V_0,V_2) = (1-p)\,[2(1-p)\gamma v_2 - 3p - (1-p)\gamma v_2 (4 - 2\gamma v_2) H(\gamma v_2)]\,.} \tag{44}$$

Figure 2(d) visualizes this asymptotic covariance.

Next we turn to $\sigma(V_1,V_1)$ as given by (19) for $n = 2$. Some of our calculations will also be required to compute $\sigma(V_0,V_1)$ and $\sigma(V_0,V_0)$. We have

$$\begin{aligned}C_1(x;\bar{h}) = \frac{a}{4} \int \mathbf{1}\{y - x \in K^0, y \in A_1^+ \cup A_1^-\}\, \mathscr{H}^1(dy) \\ + \frac{b}{4} \int \mathbf{1}\{y - x \in K^0, y \in A_2^+ \cup A_2^-\}\, \mathscr{H}^1(dy)\end{aligned}$$

and a straightforward calculation (left to the reader) yields

$$C_1(x;\bar{h}) = \mathbf{1}\{|x_1| \le a, |x_2| \le b\} \Big(\frac{a}{4}(b - |x_2|) + \frac{b}{4}(a - |x_1|) \Big) \tag{45}$$

as well as

$$C_1(x) = \frac{1}{2} \mathbf{1}\{|x_1| \le a, |x_2| \le b\} ((a - |x_1|) + (b - |x_2|)).$$

From $C_1(x;\bar{h}) = C_1(-x;\bar{h})$ (see (45)) and (39) (with $f(x) := e^{\gamma C_2(x)}$ and $\tilde{f} \equiv 1$) it follows that

$$\int e^{\gamma C_2(y-z)} C_1(y - z;\bar{h})\, N_{1,2}(d(z,u,y)) = J_1 + J_2,$$

where

$$J_1 := \frac{a}{8} \int_{[-a,a]\times[-b,b]} e^{\gamma(a-|z_1|)(b-|z_2|)} ((a - |z_1|) + (b - |z_2|))(b - |z_2|)\, d(z_1,z_2)$$

and J_2 is defined similarly. We have

$$\begin{aligned} J_1 &= \frac{a}{2}\int \mathbf{1}\{0\le z_1\le a, 0\le z_2\le b\} e^{\gamma z_1 z_2}(z_1+z_2) z_2\, d(z_1,z_2)\\ &= \frac{a^2b^2}{2}\int_0^1\int_0^1 e^{\gamma abst}(as+bt)t\,ds\,dt\\ &= \frac{a^3b^2}{2}\int_0^1\int_0^1 e^{\gamma abst} st\,ds\,dt + \frac{a^2b^3}{2}\int_0^1\int_0^1 e^{\gamma abst}t^2\,ds\,dt. \end{aligned}$$

Together with the analogous formula for J_2 this yields

$$\int e^{\gamma C_2(y-z)} C_1(y-z;\bar{h})\, N_{1,2}(d(z,u,y)) = \frac{v_1 v_2^2}{2}\int_0^1\int_0^1 e^{\gamma v_2 st}(st+t^2)\,ds\,dt.$$

Now we can use (38) with $r=\gamma v_2$ to obtain

$$\begin{aligned} &\int e^{\gamma C_2(y-z)} C_1(y-z;\bar{h})\, N_{1,2}(d(z,u,y))\\ &\qquad = \frac{v_1}{\gamma^2}e^{\gamma v_2} - \frac{v_1}{2\gamma^3 v_2}e^{\gamma v_2} + \frac{v_1}{2\gamma^3 v_2} - \frac{v_1}{2\gamma^2} - \frac{3v_1v_2}{4\gamma} - \frac{v_1v_2}{2\gamma}H(\gamma v_2). \end{aligned} \tag{46}$$

Similarly,

$$\begin{aligned} &\int e^{\gamma C_2(y-z)} C_1(y-z)\, N_{1,2}(d(z,u,y))\\ &\qquad = \int \mathbf{1}\{0\le z_1\le a, 0\le z_2\le b\} e^{\gamma z_1 z_2}(z_1+z_2)^2\, d(z_1,z_2)\\ &\qquad = ab\int_0^1\int_0^1 e^{\gamma abst}(as+bt)^2\,ds\,dt\\ &\qquad = ab(a^2+b^2)\int_0^1\int_0^1 e^{\gamma abst}s^2\,ds\,dt + 2a^2b^2\int_0^1\int_0^1 e^{\gamma abst} st\,ds\,dt. \end{aligned}$$

It follows from (36) and (37) that the latter sum equals

$$\begin{aligned} &ab(a^2+b^2)\Big(\frac{1}{\gamma^2a^2b^2}e^{\gamma v_2} - \frac{1}{\gamma^3a^3b^3}e^{\gamma v_2} + \frac{1}{\gamma^3a^3b^3} - \frac{1}{2\gamma ab}\Big)\\ &\quad + 2a^2b^2\Big(\frac{1}{\gamma^2a^2b^2}e^{\gamma ab} - \frac{1}{\gamma^2a^2b^2} - \frac{1}{\gamma ab}H(\gamma ab) - \frac{1}{\gamma ab}\Big). \end{aligned}$$

Therefore

$$\begin{aligned} &\gamma^2\int e^{\gamma C_2(y-z)} C_1(y-z)\, N_{1,2}(d(z,u,y))\\ &\quad = (a^2+b^2)\Big(\frac{1}{v_2}e^{\gamma v_2} - \frac{1}{\gamma v_2^2}e^{\gamma v_2} + \frac{1}{\gamma v_2^2} - \frac{\gamma}{2}\Big) + 2e^{\gamma v_2} - 2 - 2v_2\gamma(H(\gamma v_2)+1). \end{aligned}$$

To proceed, we need to compute the integrals

$$I_1^{++} := \int \mathbf{1}\{y\in A_1^+, z\in A_1^+\} e^{\gamma C_2(y-z)}\,\mathscr{H}^1(dy)\,\mathscr{H}^1(dz), \tag{47}$$

$$I_1^{+-} := \int \mathbf{1}\{y \in A_1^+, z \in A_1^-\} e^{\gamma C_2(y-z)} \mathscr{H}^1(dy)\mathscr{H}^1(dz),$$
$$I_{1,2}^{+} := \int \mathbf{1}\{y \in A_1^+, z \in A_2^+\} e^{\gamma C_2(y-z)} \mathscr{H}^1(dy)\mathscr{H}^1(dz) \tag{48}$$

as well as I_2^{++} (resp. I_2^{+-}), arising from I_1^{++} (resp. I_1^{+-}) by replacing (A_1^+, A_1^+) (resp. (A_1^+, A_1^-)) with (A_2^+, A_2^+) (resp. (A_2^+, A_2^-)). A straightforward calculation gives

$$I_1^{++} = \frac{2b}{\gamma a} e^{\gamma ab} - \frac{2}{\gamma^2 a^2} e^{\gamma ab} + \frac{2}{\gamma^2 a^2}, \qquad I_2^{++} = \frac{2a}{\gamma b} e^{\gamma ab} - \frac{2}{\gamma^2 b^2} e^{\gamma ab} + \frac{2}{\gamma^2 b^2}, \tag{49}$$
$$I_1^{+-} = b^2, \qquad I_2^{+-} = a^2, \tag{50}$$
$$I_{1,2}^{+} = ab(H(\gamma ab) + 1). \tag{51}$$

We prove here (49). The proof of (50) and (51) is even simpler. By the parametrisation $y = (a/2, s)$ with $s \in [-b/2, b/2]$ for $y \in A_1^+$ and $z = (a/2, t)$ with $t \in [-b/2, b/2]$ for $z \in A_2^+$ we get

$$I_1^{++} = \int_{-b/2}^{b/2} \int_{-b/2}^{b/2} e^{\gamma a(b - |s-t|)}\, ds\, dt.$$

Splitting the domain of integration into $s < t$ and $s \geq t$ yields

$$\begin{aligned} I_1^{++} &= 2e^{\gamma ab} \int_{-b/2}^{b/2} e^{\gamma at} \int_t^{b/2} e^{-\gamma as}\, ds\, dt \\ &= \frac{2}{\gamma a} e^{\gamma ab} \int_{-b/2}^{b/2} \left(1 - e^{-\gamma ab/2} e^{\gamma at}\right) dt. \end{aligned}$$

Continuing this calculation gives

$$I_1^{++} = \frac{2b}{\gamma a} e^{\gamma ab} - \frac{2}{\gamma^2 a^2} e^{\gamma ab/2} \left(e^{\gamma ab/2} - e^{-\gamma ab/2}\right)$$

and hence the first identity in (49). The second follows by symmetry.

By symmetry arguments we have

$$\int e^{\gamma C_2(x-y)} N_{1,1}(d(x,u,y,v)) = 2\frac{1}{4} I_1^{++} + 2\frac{1}{4} I_2^{++} + 2\frac{1}{4} I_1^{+-} + 2\frac{1}{4} I_2^{+-} + 8\frac{1}{4} I_{1,2}^{+},$$

so that (49)–(51) yield

$$\begin{aligned} \int e^{\gamma C_2(x-y)} N_{1,1}(d(x,u,y,v)) &= \frac{b}{\gamma a} e^{\gamma ab} - \frac{1}{\gamma^2 a^2} e^{\gamma ab} + \frac{1}{\gamma^2 a^2} \\ &\quad + \frac{a}{\gamma b} e^{\gamma ab} - \frac{1}{\gamma^2 b^2} e^{\gamma ab} + \frac{1}{\gamma^2 b^2} + \frac{a^2 + b^2}{2} + 2ab(H(\gamma ab) + 1). \end{aligned}$$

Therefore,

$$\gamma\int e^{\gamma C_2(x-y)}N_{1,1}(d(x,u,y,v))$$
$$=\frac{a^2+b^2}{v_2}e^{\gamma v_2}-\frac{a^2+b^2}{\gamma v_2^2}e^{\gamma v_2}+\frac{a^2+b^2}{\gamma v_2^2}+\gamma\frac{a^2+b^2}{2}+2\gamma v_2(H(\gamma v_2)+1),$$

so that

$$\begin{aligned}&\gamma^2\int e^{\gamma C_2(y-z)}C_1(y-z)N_{1,2}(d(z,u,y))+\gamma\int e^{\gamma C_2(x-y)}N_{1,1}(d(x,u,y,v))\\&=(a^2+b^2)\Big(\frac{1}{v_2}e^{\gamma v_2}-\frac{1}{\gamma v_2^2}e^{\gamma v_2}+\frac{1}{\gamma v_2^2}-\frac{\gamma}{2}\Big)+2e^{\gamma v_2}-2\\&\quad+\frac{a^2+b^2}{v_2}e^{\gamma v_2}-\frac{a^2+b^2}{\gamma v_2^2}e^{\gamma v_2}+\frac{a^2+b^2}{\gamma v_2^2}+\gamma\frac{a^2+b^2}{2}\\&=2(a^2+b^2)\Big(\frac{1}{v_2}e^{\gamma v_2}-\frac{1}{\gamma v_2^2}e^{\gamma v_2}+\frac{1}{\gamma v_2^2}\Big)+2e^{\gamma v_2}-2.\end{aligned}$$

Now we can conclude from (19), (32) and (41) that

$$\begin{aligned}\sigma(V_1,V_1)&=4(1-p)^2\gamma^2v_1^2v_2H(\gamma v_2)-4(1-p)^2v_1^2\gamma^2\left(\frac{1}{\gamma^2v_2}e^{\gamma v_2}-\frac{1}{\gamma^2v_2}-\frac{1}{\gamma}\right)\\&\quad+(1-p)^2 2(a^2+b^2)\Big(\frac{1}{v_2}e^{\gamma v_2}-\frac{1}{\gamma v_2^2}e^{\gamma v_2}+\frac{1}{\gamma v_2^2}\Big)+(1-p)^2(2e^{\gamma v_2}-2),\end{aligned}$$

that is

$$\boxed{\begin{aligned}\sigma(V_1,V_1)=(1-p)\Big[&2p+4(1-p)\gamma^2v_1^2v_2H(\gamma v_2)\\&-4\gamma^2v_1^2\left(\frac{p}{\gamma^2v_2}-\frac{1-p}{\gamma}\right)+2(a^2+b^2)\Big(\frac{1}{v_2}-\frac{p}{\gamma v_2^2}\Big)\Big],\end{aligned}} \tag{52}$$

which is shown in Fig. 2(c).

We now turn to $\sigma(V_0,V_1)$. It follows from (46) that

$$\begin{aligned}&-2\gamma^3\int e^{\gamma C_2(y-z)}C_1(y-z;\bar{h})N_{1,2}(d(z,u,y))\\&\quad=-2\gamma v_1e^{\gamma v_2}+\frac{v_1}{v_2}e^{\gamma v_2}-\frac{v_1}{v_2}+\gamma v_1+\frac{3\gamma^2v_1v_2}{2}+\gamma^2v_1v_2H(\gamma v_2).\end{aligned}$$

Furthermore we have from (41) and $v_{1,1}=v_2$

$$\begin{aligned}&(\gamma^3v_{1,1}-\gamma^2)\int e^{\gamma C_2(y-z)}N_{1,2}(d(z,u,y))\\&\quad=2v_1\gamma^3v_2\left(\frac{1}{\gamma^2v_2}e^{\gamma v_2}-\frac{1}{\gamma^2v_2}-\frac{1}{\gamma}\right)-2v_1\gamma^2\left(\frac{1}{\gamma^2v_2}e^{\gamma v_2}-\frac{1}{\gamma^2v_2}-\frac{1}{\gamma}\right)\end{aligned}$$

$$= 2\gamma v_1 e^{\gamma v_2} - 2\gamma v_1 - 2\gamma^2 v_1 v_2 - \frac{2v_1}{v_2} e^{\gamma v_2} + \frac{2v_1}{v_2} + 2\gamma v_1.$$

Further we have from (43) and $\overline{\Psi}(1) = v_1$

$$\begin{aligned} 2\gamma^3 \overline{\Psi}_1(1) \int e^{\gamma C_2(y-z)} \bar{h}(u) N_{1,2}(d(z,u,y)) &= 2\gamma^3 v_1 \Big(\frac{2}{\gamma^2} e^{\gamma v_2} - \frac{2}{\gamma^2} - \frac{2v_2}{\gamma} \Big) \\ &= 4\gamma v_1 e^{\gamma v_2} - 4\gamma v_1 - 4\gamma^2 v_1 v_2. \end{aligned}$$

Summarizing the previous formulae we arrive at

$$\begin{aligned} &(1-p)^2 \int \big(\chi'(y-z) + 2\gamma^3 \overline{\Psi}_1(1) e^{\gamma C_2(y-z)} \bar{h}(u) \big) N_{1,2}(d(z,u,y)) \\ &\quad = (1-p)\gamma v_1 \left[1 + \left(3 - \frac{1}{\gamma v_2} \right) p + (1-p)\gamma v_2 \left(H(\gamma v_2) - \frac{9}{2} \right) \right]. \end{aligned} \tag{53}$$

Next we consider

$$I := \int e^{\gamma C_2(y-z)} \bar{h}(u) N_{1,1}(d(y,u,z,v)).$$

Then $I = I_1 + I_2$, where

$$\begin{aligned} I_1 &:= \frac{a}{8} \int \mathbf{1}\{y \in A_1^+ \cup A_1^-\} e^{\gamma C_2(y-z)} \mathscr{H}^1(dy) \mathscr{H}^1(dz), \\ I_2 &:= \frac{b}{8} \int \mathbf{1}\{y \in A_2^+ \cup A_2^-\} e^{\gamma C_2(y-z)} \mathscr{H}^1(dy) \mathscr{H}^1(dz). \end{aligned}$$

By symmetry,

$$I_1 = 2\frac{a}{8} I_1^{++} + 2\frac{a}{8} I_1^{+-} + 4\frac{a}{8} I_{1,2}^{+}, \quad I_2 = 2\frac{b}{8} I_2^{++} + 2\frac{b}{8} I_2^{+-} + 4\frac{a}{8} I_{1,2}^{+},$$

where the occurring integrals have been defined by (47)–(48). The formulae (49)–(51) yield

$$\begin{aligned} I = &\Big(\frac{a}{2\gamma} + \frac{b}{2\gamma} \Big) e^{\gamma ab} - \Big(\frac{1}{2\gamma^2 a} + \frac{1}{2\gamma^2 b} \Big) e^{\gamma ab} + \frac{1}{2\gamma^2 a} + \frac{1}{2\gamma^2 b} \\ &+ \frac{ab^2}{4} + \frac{a^2 b}{4} + \Big(\frac{a^2 b}{2} + \frac{ab^2}{2} \Big) (H(\gamma ab) + 1), \end{aligned}$$

that is

$$I = \frac{v_1}{2\gamma} e^{\gamma v_2} - \frac{v_1}{2\gamma^2 v_2} e^{\gamma v_2} + \frac{v_1}{2\gamma^2 v_2} + \frac{3v_1 v_2}{4} + \frac{v_1 v_2}{2} H(\gamma v_2).$$

It follows that

$$-2(1-p)^2\gamma^2\int e^{\gamma C_2(y-z)}\overline{h}(u)\,N_{1,1}(d(y,u,z,v))$$
$$=(1-p)\gamma\nu_1\left[\frac{p}{\gamma\nu_2}-1-\left(\frac{3}{2}+H(\gamma\nu_2)\right)(1-p)\gamma\nu_2\right]. \tag{54}$$

Now we conclude from (21) and (32) that

$$\sigma(V_0,V_1)=(1-p)\gamma\nu_1\left[1-p+4(1-p)\gamma\nu_2(1-\gamma\nu_2)H(\gamma\nu_2)\right]+c_{1,2}+c_{1,1},$$

where $c_{1,2}$ is given by the right-hand side of (53) and $c_{1,1}$ is given by the right-hand side of (54). Thus, we derive

$$\boxed{\sigma(V_0,V_1)=(1-p)\gamma\nu_1\left[1+2p+(1-p)\gamma\nu_2(4(1-\gamma\nu_2)H(\gamma\nu_2)-6)\right].} \tag{55}$$

The asymptotic covariance is plotted in Fig. 2(f).

Finally, we determine $\sigma(V_0,V_0)$, as given by (22). From (39) and (45) we get

$$\begin{aligned}
&\int e^{\gamma C_2(y-z)}C_1(y-z;\overline{h})\overline{h}(u)\,N_{1,2}(d(z,u,y))\\
&=\frac{a}{4}\int\mathbf{1}\{|z_1|\le a,|z_2|\le b\}e^{\gamma|z_1||z_2|}|z_2|\Big(\frac{a}{4}|z_2|+\frac{b}{4}|z_1|\Big)\,d(z_1,z_2)\\
&\quad+\frac{b}{4}\int\mathbf{1}\{|z_1|\le a,|z_2|\le b\}e^{\gamma|z_1||z_2|}|z_1|\Big(\frac{a}{4}|z_2|+\frac{b}{4}|z_1|\Big)\,d(z_1,z_2)\\
&=\frac{a}{4}\int_0^b\int_0^a e^{\gamma z_1z_2}z_2(az_2+bz_1)\,dz_1\,dz_2+\frac{b}{4}\int_0^b\int_0^a e^{\gamma z_1z_2}z_1(az_2+bz_1)\,dz_1\,dz_2\\
&=\frac{a^2b^2}{4}\int_0^1\int_0^1 e^{\gamma abst}t(abt+abs)\,ds\,dt+\frac{a^2b^2}{4}\int_0^1\int_0^1 e^{\gamma abst}s(abt+abs)\,ds\,dt\\
&=\frac{a^3b^3}{2}\int_0^1\int_0^1 e^{\gamma abst}(s^2+st)\,ds\,dt.
\end{aligned}$$

Using now (38), we obtain

$$4\gamma^4\int e^{\gamma C_2(y-z)}C_1(y-z;\overline{h})\overline{h}(u)\,N_{1,2}(d(z,u,y))$$
$$=4\gamma^2\nu_2e^{\gamma\nu_2}-2\gamma e^{\gamma\nu_2}+2\gamma-2\gamma^2\nu_2-3\gamma^3\nu_2^2-2\gamma^3\nu_2^2H(\gamma\nu_2).$$

From (43)

$$(-4\gamma^4\nu_2+4\gamma^3)\int e^{\gamma C_2(y-z)}\overline{h}(u)\,N_{1,2}(d(z,u,y))$$
$$=(-4\gamma^4\nu_2+4\gamma^3)\Big(\frac{2}{\gamma^2}e^{\gamma\nu_2}-\frac{2}{\gamma^2}-\frac{2\nu_2}{\gamma}\Big)$$
$$=-8\gamma^2\nu_2e^{\gamma\nu_2}+8\gamma^2\nu_2+8\gamma^3\nu_2^2+8\gamma e^{\gamma\nu_2}-8\gamma-8\gamma^2\nu_2.$$

Summarizing, we have

$$(1-p)^2\int \overline{h}(u)\chi''(y-z)\,N_{1,2}(d(z,u,y)) = (1-p)\gamma[6p-4\gamma\nu_2+(1-p)\gamma\nu_2(5\gamma\nu_2-2H(\gamma\nu_2)\gamma\nu_2-2)] \quad (56)$$

Next we note that

$$\int e^{\gamma C_2(y-z)}\overline{h}(u)\overline{h}(v)\,N_{1,1}(d(y,u,z,v)) = 2\frac{a^2}{16}I_1^{++}+2\frac{a^2}{16}I_1^{+-}+2\frac{b^2}{16}I_2^{++}+2\frac{b^2}{16}I_2^{+-}+8\frac{ab}{16}I_{1,2}^{+},$$

where $I_1^{++},I_1^{+-},I_{1,2}^{+},I_2^{++},I_2^{+-}$ have been defined by (47)–(48). The formulae (49)–(51) give

$$\begin{aligned}&\int e^{\gamma C_2(y-z)}\overline{h}(u)\overline{h}(v)\,N_{1,1}(d(y,u,z,v))\\ &=\frac{a^2}{8}\Big(\frac{2b}{\gamma a}e^{\gamma ab}-\frac{2}{\gamma^2a^2}e^{\gamma ab}+\frac{2}{\gamma^2a^2}\Big)+\frac{a^2b^2}{8}+\frac{b^2}{8}\Big(\frac{2a}{\gamma b}e^{\gamma ab}-\frac{2}{\gamma^2b^2}e^{\gamma ab}+\frac{2}{\gamma^2b^2}\Big)\\ &\quad+\frac{a^2b^2}{8}+\frac{a^2b^2}{2}(H(\gamma ab)+1)\\ &=\frac{\nu_2}{2\gamma}e^{\gamma\nu_2}-\frac{1}{2\gamma^2}e^{\gamma\nu_2}+\frac{1}{2\gamma^2}+\frac{\nu_2^2}{4}+\frac{\nu_2^2}{2}H(\gamma\nu_2)+\frac{\nu_2^2}{2}.\end{aligned}$$

Therefore

$$4(1-p)^2\gamma^3\int e^{\gamma C_2(y-z)}\overline{h}(u)\overline{h}(v)\,N_{1,1}(d(y,u,z,v)) = (1-p)\gamma\left[(2H(\gamma\nu_2)+3)(1-p)(\gamma\nu_2)^2+2\gamma\nu_2-2p\right]. \quad (57)$$

Now we conclude from (22) and (32) that

$$\sigma(V_0,V_0) = (1-p)\gamma[1-2p+(2p-3)\gamma\nu_2 + 4(1-p)(1-\gamma\nu_2)^2\gamma\nu_2H(\gamma\nu_2)\big]+d_{1,2}+d_{1,1},$$

where $d_{1,2}$ is given by the right-hand side of (56) and $d_{1,1}$ is given by the right-hand side of (57). Thus, we finally derive

$$\boxed{\begin{aligned}\sigma(V_0,V_0) = (1-p)\gamma[1+2p+(4p-7)\gamma\nu_2 \\ +4(1-p)\gamma\nu_2\left(2\gamma\nu_2+(1-\gamma\nu_2)^2H(\gamma\nu_2)\right)\big],\end{aligned}} \quad (58)$$

which is plotted in Fig. 2(e).

The reader might have noticed that the asymptotic covariances $\sigma(V_i,V_j)$ (with the exception of $\sigma(V_1,V_1)$) depend on the parameters γ, ν_1, and ν_2 in a specific way. In order to explain these invariance properties, let $Z_{a,b,\gamma}$ denote the Boolean model with grains $K=[0,a]\times[0,b]$ and intensity γ. By applying to each rectangle of the underlying Poisson process the linear transformation $T_{a,b}:\mathbb{R}^2\to\mathbb{R}^2,(x_1,x_2)\mapsto$

(ax_1, bx_2), one obtains the distributional identity

$$Z_{a,b,\gamma} \stackrel{d}{=} T_{a,b} Z_{1,1,ab\gamma}.$$

Together with the fact that $V_i(T_{a,b}A) = (ab)^{i/2} V_i(A)$, for $A \in \mathscr{R}^2$ and $i \in \{0,2\}$, we see that

$$\begin{aligned}
\sigma(V_i, V_j) &= \lim_{r(W)\to\infty} \frac{\mathbf{cov}(V_i(Z_{a,b,\gamma} \cap W), V_j(Z_{a,b,\gamma} \cap W))}{V_2(W)} \\
&= \lim_{r(W)\to\infty} \frac{\mathbf{cov}(V_i(T_{a,b} Z_{1,1,ab\gamma} \cap W), V_j(T_{a,b} Z_{1,1,ab\gamma} \cap W))}{V_2(W)} \\
&= (ab)^{i/2+j/2-1} \lim_{r(W)\to\infty} \frac{\mathbf{cov}(V_i(Z_{1,1,ab\gamma} \cap T_{a,b}^{-1} W), V_j(Z_{1,1,ab\gamma} \cap T_{a,b}^{-1} W))}{V_2(T_{a,b}^{-1} W)} \\
&= \nu_2^{i/2+j/2-1} \lim_{r(W)\to\infty} \frac{\mathbf{cov}(V_i(Z_{1,1,\gamma\nu_2} \cap W), V_j(Z_{1,1,\gamma\nu_2} \cap W))}{V_2(W)},
\end{aligned}$$

for $i, j \in \{0,2\}$. This shows that for all Boolean models of deterministic rectangles with fixed $\gamma\nu_2$, the asymptotic covariances between volume and Euler characteristic are a power of ν_2 times a constant depending on $\gamma\nu_2$.

Next we investigate the invariance properties of $\sigma(V_0, V_1)$ and $\sigma(V_1, V_2)$. For $i \in \{1,2\}$ we define

$$V_{1,e_i}(A) := \int \mathbf{1}\{u = \pm e_i\}\, \Psi_1(A; du), \quad A \in \mathscr{R}^2,$$

which are again geometric functionals. If W is a rectangle with sides in the directions e_1 and e_2, which we can assume in the following, we have that

$$V_1(Z_{a,b,\gamma} \cap W) = V_{1,e_1}(Z_{a,b,\gamma} \cap W) + V_{1,e_2}(Z_{a,b,\gamma} \cap W).$$

By the same arguments as in the previous computation we obtain that, for $i \in \{0,2\}$,

$$\begin{aligned}
\sigma(V_i, V_1) &= \lim_{r(W)\to\infty} \frac{\mathbf{cov}(V_i(Z_{a,b,\gamma} \cap W), V_1(Z_{a,b,\gamma} \cap W))}{V_2(W)} \\
&= \lim_{r(W)\to\infty} \left\{ \frac{\mathbf{cov}(V_i(T_{a,b} Z_{1,1,ab\gamma} \cap W), V_{1,e_1}(T_{a,b} Z_{1,1,ab\gamma} \cap W))}{V_2(W)} \right. \\
&\qquad \left. + \frac{\mathbf{cov}(V_i(T_{a,b} Z_{1,1,ab\gamma} \cap W), V_{1,e_2}(T_{a,b} Z_{1,1,ab\gamma} \cap W))}{V_2(W)} \right\} \\
&= \lim_{r(W)\to\infty} \left\{ (ab)^{i/2-1} a \frac{\mathbf{cov}(V_i(Z_{1,1,ab\gamma} \cap W), V_{1,e_1}(Z_{1,1,ab\gamma} \cap W))}{V_2(W)} \right. \\
&\qquad \left. + (ab)^{i/2-1} b \frac{\mathbf{cov}(V_i(Z_{1,1,ab\gamma} \cap W), V_{1,e_2}(Z_{1,1,ab\gamma} \cap W))}{V_2(W)} \right\}.
\end{aligned}$$

Using that the asymptotic covariances between V_i and V_{1,e_1} and between V_i and V_{1,e_2} are the same for the Boolean model $Z_{1,1,ab\gamma}$ due to symmetry, we conclude that

$$\begin{aligned}\sigma(V_i,V_1) &= \lim_{r(W)\to\infty}(ab)^{i/2-1}(a+b)\frac{\mathbf{cov}(V_i(Z_{1,1,ab\gamma}\cap W),V_{1,e_1}(Z_{1,1,ab\gamma}\cap W))}{V_2(W)}\\ &= \lim_{r(W)\to\infty}\left\{(ab)^{i/2-1}\frac{(a+b)}{2}\frac{\mathbf{cov}(V_i(Z_{1,1,ab\gamma}\cap W),V_{1,e_1}(Z_{1,1,ab\gamma}\cap W))}{V_2(W)}\right.\\ &\qquad\left.+(ab)^{i/2-1}\frac{(a+b)}{2}\frac{\mathbf{cov}(V_i(Z_{1,1,ab\gamma}\cap W),V_{1,e_2}(Z_{1,1,ab\gamma}\cap W))}{V_2(W)}\right\}\\ &= \lim_{r(W)\to\infty}v_2^{i/2-1}\frac{v_1}{2}\frac{\mathbf{cov}(V_i(Z_{1,1,\gamma v_2}\cap W),V_1(Z_{1,1,\gamma v_2}\cap W))}{V_2(W)}.\end{aligned}$$

Thus, the asymptotic covariance between volume and surface area is v_1 times a constant depending on γv_2, while the covariance between Euler characteristic and surface area is $v_1 v_2^{-1}$ times a constant depending on γv_2.

Figure 2 summarizes the results of this section visually. It shows the asymptotic covariances $\sigma(V_i,V_j)$ as a function of the intensity γ for Boolean models of aligned rectangles for a variety of aspect ratios b/a.

6 Simulations of Boolean models with isotropic or aligned rectangles

Planar Boolean models with either squares or rectangles with aspect ratio $1/2$ as grains are simulated in a finite observation window. We study the variances and covariances of the intrinsic volumes as well as their relative frequency histograms weighted by the size of each bin. We compare the simulation results for aligned rectangles to the analytic formulae for the covariances in the previous Section 5. Moreover, we simulate rectangles with a uniform (isotropic) orientation distribution and find, e.g., for $\sigma(V_0,V_1)$ a qualitatively different behaviour.

Tensor valuation densities and the density of the Euler characteristic $\overline{V}_0$ of anisotropic Boolean models are studied in [13]. The same simulation procedure is applied here with even better statistics for reliable estimates of the second moments and the histograms of the intrinsic volumes.

The grain centres are random points, uniformly distributed within the simulation box. The union of the rectangles is computed using the Computational Geometry Algorithms Library (CGAL) [5]. The program PAPAYA then calculates the Minkowski functionals of the Boolean model [41].

For aligned rectangles, the covariances $\sigma(V_2,V_2)$, $\sigma(V_0,V_0)$, and $\sigma(V_0,V_2)$ as well as the rescaled covariances $\sigma(V_1,V_2)/(2a+2b)$ and $\sigma(V_0,V_1)/(2a+2b)$ are only functions of v_2 and γv_2, as shown in the previous Section 5. In other words, if the unit of area is chosen to be the area of a single grain $v_2 = a\cdot b = 1$ (so that the area of the typical grain does not depend on the aspect ratio), the rescaled covariances

are independent of the aspect ratio. Therefore, we define in the following the unit of length by the square root of the area of a single grain.

Parts of this section are taken from the PhD thesis of one of the authors [19].

6.1 Variances and covariances

The first moments of area or perimeter of a Boolean model are rather insensitive to the grain distribution. Indeed, if the unit of area is chosen to be the mean area of a single grain, the density of the area, i.e., the occupied area fraction, of the Boolean model is only a function of the intensity. Moreover, if the density of the perimeter in the asymptotic limit is divided by the mean perimeter of a single grain, it is also independent of the grain distribution [39, Theorem 9.1.4.].

Does the same hold for the second moments? Is there a qualitatively different behaviour in the variances and covariances depending on whether the orientation distribution of the grains is isotropic or anisotropic? Which covariances or variances are invariant under affine transformations of the grain distributions?

Depending on the computational costs, for each different set of parameters we perform between $M_s = 21{,}000$ and $600{,}000$ simulations of Boolean models with rectangles: at varying intensities γ, with aspect ratio 1 or $1/2$, and for rectangles either aligned w.r.t. the observation window or with an isotropic orientation distribution. The simulation box is a square with side length $L = 4a$, where periodic boundary conditions are applied. The number of grains within the simulation box is a random number and follows a Poisson distribution with mean $\gamma \cdot L^2$. To estimate the covariances, we simulate more than $5{,}800{,}000$ samples of Boolean models including about $54{,}000{,}000$ rectangles in total.

Because of the periodic boundary conditions, the covariances of this system coincide with the asymptotic covariances for the infinite volume system from Section 5, as we have pointed out in Subsection 3.3.

For each sample $m \in \{1, \dots M_s\}$ of a Boolean model, we determine the intrinsic volumes $V_i^{(m)}$ ($i = 0, 1, 2$). The sample covariance then provides an estimate for the covariance between the Minkowski functionals:

$$s(V_i, V_j) := \frac{1}{M_s - 1} \sum_{m=1}^{M_s} (V_i^{(m)} - \langle V_i \rangle)(V_j^{(m)} - \langle V_j \rangle)$$

using the sample mean $\langle V_i \rangle := \frac{1}{M_s} \sum_{m=1}^{M_s} V_i^{(m)}$ as an estimator for the expectation. In accordance with the definition of the asymptotic covariances in Theorem 1, the sample covariance is then divided by the size L^2 of the observation window. We finally use bootstrapping (with 1000 bootstrap samples) to estimate the mean and the error of the estimators.

Figure 3 shows the simulation results for the variances and covariances of the intrinsic volumes for an isotropic orientation distribution of the grains as well as for aligned rectangles. In the latter case, the simulation results are compared to the

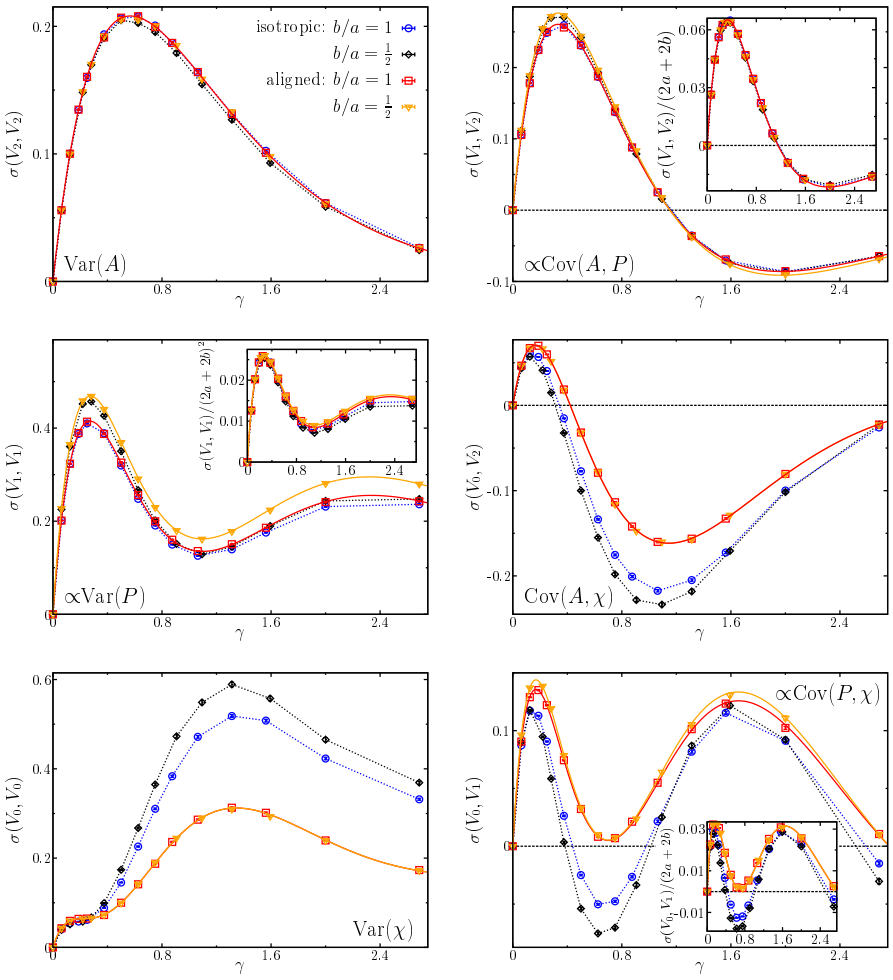

Fig. 3 Variances and covariances of the intrinsic volumes V_2 (area A), V_1 (proportional to perimeter P), and V_0 (Euler characteristic χ) of Boolean models as a function of the intensity γ. Depicted are both numerical estimates in finite observation windows with periodic boundary conditions (marks with dotted lines as guides to the eye) and analytic curves of the covariances (solid lines), see Eqs. (34), (42), (44), (52), (55), and (58). Four different Boolean models are simulated: both for squares ($b/a = 1$) and rectangles ($b/a = 1/2$) either an isotropic orientation distribution is used or the grains are aligned with the x-direction. In the insets, the covariances and the variance of the perimeter of the Boolean model are rescaled by the perimeter of a single grain. In contrast to Fig. 2, the unit of area is the size of a single grain, that is $v_2 = ab = 1$.

analytic results in Eqs. (34), (42), (44), (52), (55), and (58). They are in excellent agreement.

The variances and covariances of the Minkowski functionals of overlapping rectangles exhibit a complex behaviour as functions of the intensity γ similar to the

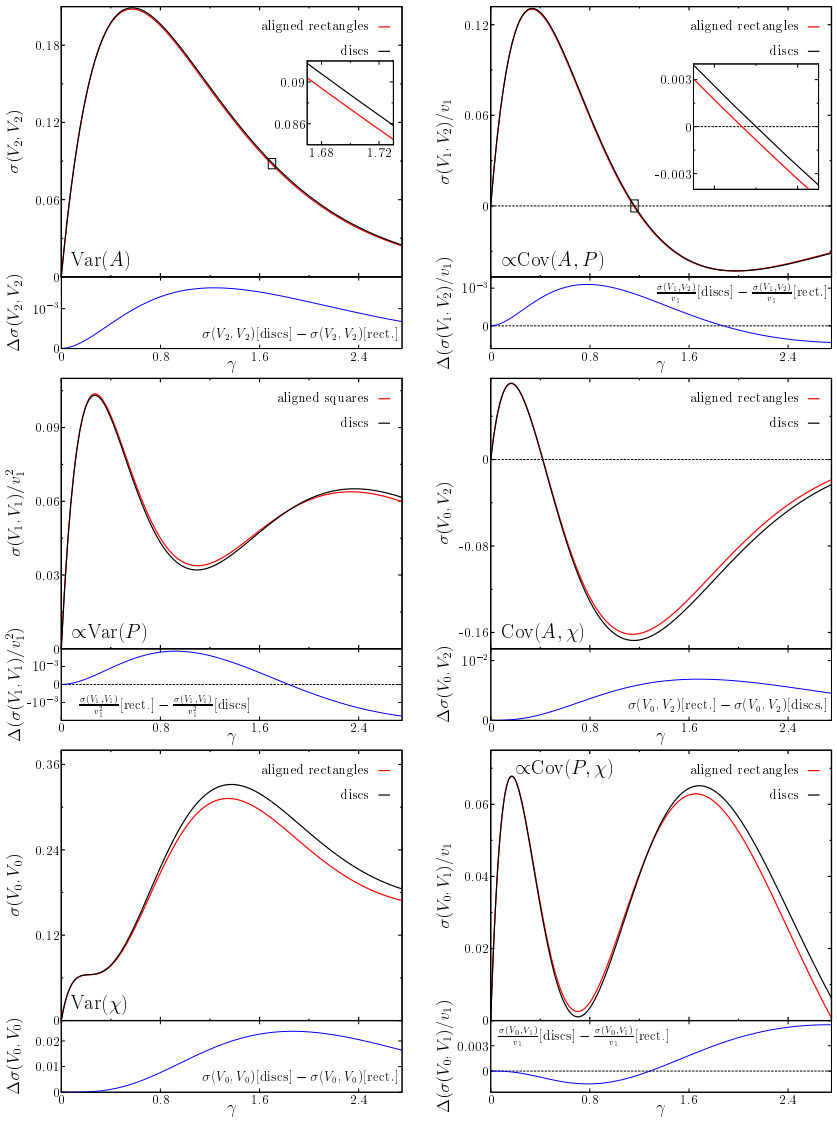

Fig. 4 Variances and covariances: $\sigma(V_2,V_2)$, the variance of the area; $\sigma(V_1,V_2)/v_1$, proportional to the covariance of area and perimeter; v_1 is half of the perimeter of a single grain; $\sigma(V_1,V_1)/v_1^2$, proportional to the variance of the perimeter; $\sigma(V_0,V_2)$, the covariance of area and Euler characteristic; $\sigma(V_0,V_0)$, the variance of the Euler characteristic; $\sigma(V_0,V_1)/v_1$, proportional to the covariance of perimeter and Euler characteristic. They are shown both for Boolean models with aligned rectangles, see Eqs. (34), (42), (44), (52), (55), and (58), and for overlapping discs, see [16]. Note that except for $\sigma(V_1,V_1)/v_1^2$ the curves for the rectangles are independent of the aspect ratio of the rectangle, see also Figs. 2 and 3. The insets in the figures at the top are close-up views which show that the covariances differ slightly for Boolean model with rectangles or with discs. Below each subfigure, the differences of the covariances for Boolean models with rectangles or discs are plotted.

Boolean model with discs in [16, Section 7]. The variances of area and Euler characteristic apparently have one maximum and no other extrema. The variance of the perimeter has a global maximum and (at least) one local minimum. As expected, the three Minkowski functionals are positively correlated at low intensities γ, but at relatively high intensities the area is anti-correlated to both the Euler characteristic and the perimeter.

The covariance $\sigma(V_0,V_1)$ between the perimeter and the Euler characteristic shows a qualitatively different behaviour for rectangles with an isotropic orientation distribution when compared to the overlapping discs or aligned rectangles. There is a regime in the intensity γ (around the first local minimum) for which the rectangles with an isotropic orientation distribution are anti-correlated, while the aligned grains are positively correlated like the discs in [16]. This is probably related to the fact that rotated rectangles can more easily form clusters with holes than aligned rectangles or discs. The zero-crossing of the expectation of the Euler characteristic χ for the rectangles with an isotropic orientation distribution is within this regime. For the aligned rectangles, the zero-crossing of the mean value of χ is at the end of this regime, see [13].

The question remains whether or not the variances and covariances of area or rescaled perimeter of the Boolean model are independent of the grain distribution like the first moments of these functionals. Equations (34) and (42) show that at least for aligned rectangles the variance $\sigma(V_2,V_2)$ as well as the covariance $\sigma(V_1,V_2)$ divided by the perimeter of a single grain $(2a+2b)$ are indeed independent of the aspect ratio. The simulation results from Fig. 3 might suggest that this could also be valid for the isotropic orientation distributions. However, the variance $\sigma(V_2,V_2)$ and the rescaled covariance $\sigma(V_1,V_2)/(2a+2b)$ do depend on the grain distribution, although only weakly for the models studied here. To show this, we evaluate Eqs. (34) and (42) numerically and compare the covariances to those of the Boolean model with discs from [16]. Figure 4 shows that there is a weak but significant difference in the analytic curves of $\sigma(V_2,V_2)$ and $\sigma(V_1,V_2)$ for the two different models. The variance of the perimeter depends more clearly on the grain distribution. Even if it is rescaled by the perimeter of a single grain and even for aligned grains, the variance distinctly depends on the aspect ratio of the rectangles (except for small intensities γ). So, in contrast to the first moments of the area and rescaled perimeter of the Boolean model, the second moments in general depend on the grain distribution, e.g., the orientation distribution, even if this dependence may be weak. As expected, also the variance $\sigma(V_0,V_0)$ of the Euler characteristic as well as the covariances $\sigma(V_0,V_1)$ and $\sigma(V_0,V_2)$ depend on the grain distribution, see Fig. 4.

6.2 Central limit theorem

We also determine the histograms of the intrinsic volumes in a finite observation window, where the histograms are weighted by the total number of samples and the bin width. The histograms are then compared to the density of a standard normal

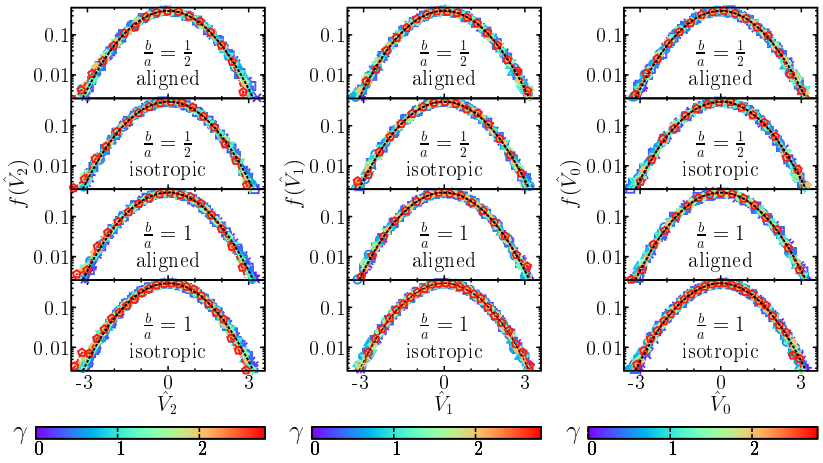

Fig. 5 Histograms f of the normalized intrinsic volumes $\hat{V}_i$ (see Eq. (59)) of Boolean models of rectangles with different aspect ratios b/a for different intensities γ; for both aligned rectangles and rectangles with an isotropic orientation distribution. For all of these different models, the rescaled distributions are already for the relatively small system size $L = 20a$ in very good agreement with a normal distribution (dashed black line).

distribution in order to numerically validate the central limit theorems in Section 4. The information content of a histogram is up to the binning almost equivalent to the empirical distribution function, but in plotting it is more convenient to compare histograms and densities.

The histograms resemble probability density functions. However, the intrinsic volumes of the considered Boolean model do not have probability density functions. Indeed, with positive probability, there is no overlap between the grains and there are no intersections with the boundary so that some multiples of the intrinsic volumes of the fixed grain have positive probability.

In this subsection, we simulate larger systems than in the previous Subsection 6.1. For a simulation box with side length $L = 20a$, we perform for each different set of parameters between $M_s = 5000$ and 150,000 simulations of Boolean models with rectangles at varying intensities γ. Like in Subsection 6.1, the rectangles have aspect ratio 1 or $1/2$, and they are either aligned w.r.t. the observation window or their orientation is isotropically distributed. To produce the histograms, we simulate more than 1,400,000 samples of Boolean models including about 350,000,000 rectangles in total.

We normalize the intrinsic volumes V_i, i.e., we subtract the estimated mean values $\langle V_i \rangle$ of the intrinsic volumes and divide by $\sqrt{s(V_i, V_i)}$:

$$\hat{V}_i := \frac{V_i - \langle V_i \rangle}{\sqrt{s(V_i, V_i)}} \,. \tag{59}$$

Figure 5 plots the histograms f of the normalized intrinsic volumes of Boolean models with different aspect ratios b/a for either aligned rectangles or rectangles with an isotropic orientation distribution and for varying intensities γ.

These histograms are in good agreement with the density function of a normal distribution for all intrinsic volumes, for all intensities, and for all of the simulated models (despite the relatively small simulation box). In other words, even in small observation windows, the probability distributions of the intrinsic volumes of Boolean models can be well approximated by Gaussian distributions.

As we have mentioned in the introduction, the central limit theorems for the geometric functionals (see Theorems 5 and 6) and the exact formulae for the second moments (see Theorems 2 and 3) can be used for hypothesis testing of models of random heterogeneous media. A hypothesis test could, e.g., use the intrinsic volumes to decide whether or not a random two-phase medium can be modeled by overlapping grains. The joint probability distribution of the Minkowski functionals allows for a characterization of the shape by several geometrical functionals and hence for a construction of tests using their full covariance structure. For a different random field (with a Poisson distributed number of counts in a binned gamma-ray sky map) such a sensitive morphometric data analysis has already been developed [8, 20]. The same concepts could be applied to the Boolean model.

In Fig. 5, there are only small deviations from a normal distribution relative to the error bars. So, the systematic deviations, e.g., due to the finite observation window size, seem to be small. In order to determine these deviations, a very high numerical accuracy is needed. We simulate $3 \cdot 10^6$ samples of two Boolean models for rectangles with aspect ratio $1/2$ that are either aligned or follow an isotropic orientation distribution. Here, we apply minus sampling boundary conditions, i.e., we consider all grains with centres in a slightly larger simulation box $[-\sqrt{a^2+b^2}/2, L+\sqrt{a^2+b^2}/2]^2$, but the observation window is still the original square $(0,L)^2$ with $L = 20a$. Contributions caused by the boundary are here neglected as it is often done in physics. The expected number of grains in the simulation box is adjusted accordingly and follows a Poisson distribution with mean $\gamma \cdot (L+\sqrt{a^2+b^2})^2$. To minimize the computational costs, a relatively low intensity γ is chosen for these simulations. It corresponds to an expected occupied area fraction $\phi = 1/15$. The resulting histograms are plotted in Fig. 6. As expected, the high statistics reveal for the small system size deviations from the normal distribution that are significantly larger than the error bars.

For each underlying Boolean model, the histograms of the normalized intrinsic volumes coincide within error bars. This is not surprising because at the low intensity chosen here the intrinsic volumes are strongly correlated. (The correlation coefficients are larger than 0.9.)

For different Boolean models (isotropic orientation distribution or aligned grains), the histogram of the non-rescaled Minkowski functionals differ slightly but distinctly already for the relatively small intensity studied here, see the inset of Fig. 6. In contrast to this, the histograms of the normalized intrinsic volumes collapse for the different Boolean models within the error bars to a single curve, which can be well approximated by a standardized Poisson distribution. This can be explained

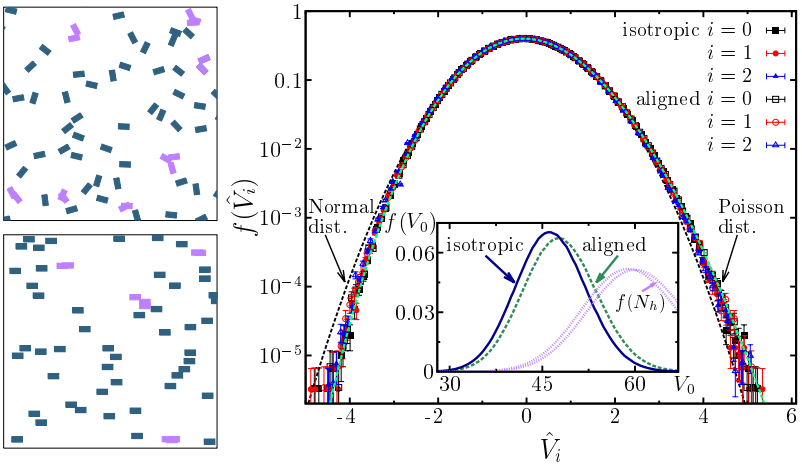

Fig. 6 Histograms f of the normalized intrinsic volumes $\hat{V}_i$ (see Eq. (59)) of Boolean models with either aligned rectangles or rectangles with an isotropic orientation distribution. The dashed black line depicts the density of a normal distribution. On the left hand side, two samples of the Boolean models with either an isotropic orientation distribution or aligned rectangles are shown; clusters of rectangles are colored purple. The inset shows the histograms of the non-rescaled Euler characteristic V_0 in the isotropic and aligned case as well as the corresponding probability mass functions of the number of grains N_h hitting the observation window with mean values 59.4 and 60.5, respectively.

by the strong correlation between the intrinsic volumes and the number of grains N_h hitting the observation window for each Boolean model. The latter follows a Poisson distribution with parameter $\mathbf{E}[N_h] = \gamma \cdot \mathbf{E}[V_2([0;L]^2 + Z_0)]$. (The correlation coefficients are larger than 0.85.) There is only a small relative difference between the parameters $\mathbf{E}[N_h]$ for the different considered Boolean models, because the observation window is large when compared to the typical grain Z_0. Therefore, the corresponding Poisson distributions are very close after standardization (dashed green line in Fig. 6) and coincide with the histograms of the normalized intrinsic volumes.

Acknowledgements We would like to thank Julia Hörrmann and Klaus Mecke for some helpful remarks and discussions. The authors were supported by the German Research Foundation (DFG) through the research unit "Geometry and Physics of Spatial Random Systems".

References

1. Arns, C., Knackstedt, M., Mecke, K.: Reconstructing complex materials via effective grain shapes. Phys. Rev. Lett. **91**, 1–4 (2003)
2. Baryshnikov, Y., Yukich, J.E.: Gaussian limits for random measures in geometric probability. Ann. Appl. Probab. **15**, 213–253 (2005)
3. Baddeley, A.: A limit theorem for statistics of spatial data. Adv. in Appl. Probab. **12**, 447–461 (1980)

4. Brodatzki, U., Mecke K.: Simulating stochastic geometries: morphology of overlapping grains. Comput. Phys. Commun. **147**, 218–221 (2002)
5. CGAL, Computational Geometry Algorithms Library. http://www.cgal.org
6. Chiu, S. N., Stoyan, D., Kendall, W. S., Mecke, J.: Stochastic Geometry and its Applications, Third Edition. Wiley, Chichester (2013)
7. Davy, P.: Projected thick sections through multi-dimensional particle aggregates. J. Appl. Probab. **13**, 714–722 (1976); Correction: J. Appl. Probab. **15**, 456 (1978)
8. Göring, D., Klatt, M. A., Stegmann, C., Mecke, K.: Morphometric analysis in gamma-ray astronomy using Minkowski functionals. Astron. Astrophys. **555**, A38 (2013)
9. Hall, P.: Introduction to the Theory of Coverage Processes. Wiley, New York (1988)
10. Heinrich, L.: Large deviations of the empirical volume fraction for stationary Poisson grain models. Ann. Appl. Probab. **15**, 392–420 (2005)
11. Heinrich, L., Molchanov, I.S.: Central limit theorems for a class of random measures associated with germ-grain models. Adv. in Appl. Probab. **31**, 283–314 (1999)
12. Hörrmann, J.: The method of densities for non-isotropic Boolean models. PhD thesis, Karlsruhe Institute of Technology (2014)
13. Hörrmann, J., Hug, D., Klatt, M. A., Mecke, K.: Minkowski tensor density formulas for Boolean models. Adv. in Appl. Math. **55**, 48–85 (2014)
14. Hörrmann, J., Weil, W., Valuations and Boolean Models. To appear in Lecture Notes in Mathematics 'Tensor Valuations and their Applications in Stochastic Geometry and Imaging', arXiv:1510.07910 (2015)
15. Hug, D.: Measures, curvatures and currents in convex geometry. Habilitationsschrift, Albert-Ludwigs-Universität Freiburg (1999)
16. Hug, D., Last, G., Schulte, M.: Second order properties and central limit theorems for geometric functionals of Boolean. Ann. Appl. Probab. **26**, 73–135 (2016)
17. Hug, D., Schneider, R.: Tensor valuations and their local versions. To appear in Lecture Notes in Mathematics 'Tensor Valuations and their Applications in Stochastic Geometry and Imaging', http://home.mathematik.uni-freiburg.de/rschnei/Tensorvaluations.Chap2.pdf (2016+)
18. Kerscher, M., Mecke, K., Schmalzing, J., Beisbart, C., Buchert, T., Wagner, H.: Morphological fluctuations of large-scale structure: The PSCz survey. Astron. Astrophys. **373**, 1–11 (2001)
19. Klatt, M. A.: Morphometry of random spatial structures in physics. PhD thesis, FAU Erlangen-Nürnberg (2016)
20. Klatt, M. A., Göring, D., Stegmann, C., Mecke, K.: Shape analysis of counts maps. AIP Conf. Proc. **1505**, 737–740 (2012)
21. Last, G., Penrose, M. D.: Fock space representation, chaos expansion and covariance inequalities for general Poisson processes. Probab. Theory Related Fields **150**, 663–690 (2011)
22. Last, G., Peccati, G., Schulte, M.: Normal approximation on Poisson spaces: Mehler's formula, second order Poincaré inequalities and stabilization. To appear in Probab. Theory Related Fields (2016+)
23. Last, G., Penrose, M. D.: Lectures on the Poisson Process. To be published by Cambridge University Press (2016+)
24. Mase, S.: Asymptotic properties of stereological estimators for stationary random sets. J. Appl. Probab. **19**, 111–126 (1982)
25. Mecke, K. R.: Additivity, convexity, and beyond: applications of Minkowski functionals in statistical physics. In: Mecke, K. R., Stoyan, D. (eds.) Statistical Physics and Spatial Statistics. Lecture Notes in Physics **554**, pp. 111–184. Springer, Berlin, Heidelberg (2000)
26. Mecke, K. R.: Exact moments of curvature measures in the Boolean model. J. Stat. Phys. **102**, 1343–1381 (2001)
27. Mecke, K. R., Buchert, T., Wagner, H.: Robust morphological measures for large-scale structure in the universe. Astron. Astrophys. **288**, 697–704 (1994)
28. Mecke, K. R., Seyfried, A.: Strong dependence of percolation thresholds on polydispersity. Europhys. Lett. **58**, 28–34 (2002)
29. Mecke, K. R., Stoyan, D.: Morphological characterization of point patterns. Biometrical J. **47**, 473–488 (2005)

30. Mecke, K., Wagner, H.: Euler characteristic and related measures for random geometric sets. J. Stat. Phys. **64**, 843–850 (1991)
31. Meester, R., Roy, R.: Continuum Percolation. Cambridge University Press, Cambridge (1996)
32. Miles, R. E.: Estimating aggregate and overall characteristics from thick sections by transmission microscopy. J. Microsc. **107**, 227–233 (1976)
33. Molchanov, I.S.: Statistics of the Boolean model: from the estimation of means to the estimation of distributions. Adv. in Appl. Probab. **21**, 63–86 (1995)
34. Molchanov, I.S.: Statistics of the Boolean Model for Practitioners and Mathematicians. Wiley, Chichester (1996)
35. Peccati, G., Solé, J. L., Taqqu, M. S., Utzet, F.: Stein's method and normal approximation of Poisson functionals. Ann. Probab. **38**, 443–478 (2010)
36. Penrose, M.D.: Gaussian limits for random geometric measures. Electron. J. Probab. **12**, 989–1035 (2007)
37. Schneider, R.: Convex Bodies: the Brunn-Minkowski Theory, Second edition. Encyclopedia of Mathematics and its Applications 151, Cambridge University Press, Cambridge (2014)
38. Schneider, R.: Valuations on convex bodies—the classical basic facts. To appear in Lecture Notes in Mathematics 'Tensor Valuations and their Applications in Stochastic Geometry and Imaging', http://home.mathematik.uni-freiburg.de/rschnei/Tensorvaluations.Chap1.pdf (2016+)
39. Schneider, R., Weil, W.: Stochastic and Integral Geometry. Springer, Berlin (2008)
40. Scholz, C., Wirner, F., Klatt, M. A., Hirneise, D., Schröder-Turk, G. E., Mecke, K., Bechinger, C.: Direct relations between morphology and transport in Boolean models. Phys. Rev. E **92**, 043023 (2015)
41. Schröder-Turk, G. E., Kapfer, S. C., Breidenbach, B., Beisbart, C., Mecke, K.: Tensorial Minkowski functionals and anisotropy measures for planar patterns. J. Microsc. **238**, 57–74 (2010)
42. Schröder-Turk, G. E., Mickel, W., Kapfer, S. C., Klatt, M. A., Schaller, F. M., Hoffmann, M. J. F., Kleppmann, N., Armstrong, P., Inayat, A., Hug, D., Reichelsdorfer, M., Peukert, W., Schwieger, W., Mecke, K.: Minkowski tensor shape analysis of cellular, granular and porous structures. Adv. Mater. **23**, 2535–2553 (2011)
43. Schröder-Turk, G. E., Mickel, W., Kapfer, S. C., Schaller, F. M., Breidenbach, B., Hug D., Mecke, K.: Minkowski tensors of anisotropic spatial structure. New J. Phys. **15**, 083028 (2013)
44. Torquato, S.: Random Heterogeneous Materials. Springer, Heidelberg (2002)